Electronic Supplementary Material (ESI) for Chemical Science.

Supplementary Information for

Regioselective phenylene-fusion reactions of Ni(II)-porphyrins controlled by an electron-withdrawing *meso*-substituent

Norihito Fukui,[a] Seung-Kyu Lee,[b] Kenichi Kato,[a] Daiki Shimizu,[a] Takayuki Tanaka,[a] Sangsu Lee,[b] Hideki Yorimitsu,*[a] Dongho Kim*[b] and Atsuhiro Osuka*[a]

[a]Department of Chemistry, Graduate School of Science, Kyoto University, Sakyo-ku, Kyoto 606-8502, Japan.

[b]Spectroscopy Laboratory of Functional π-Electronic Systems and Department of Chemistry, Yonsei University, Seoul 120-749, Korea.

Contents

1. Possible Isomers as Doubly Phenylene-Fused Porphyrins

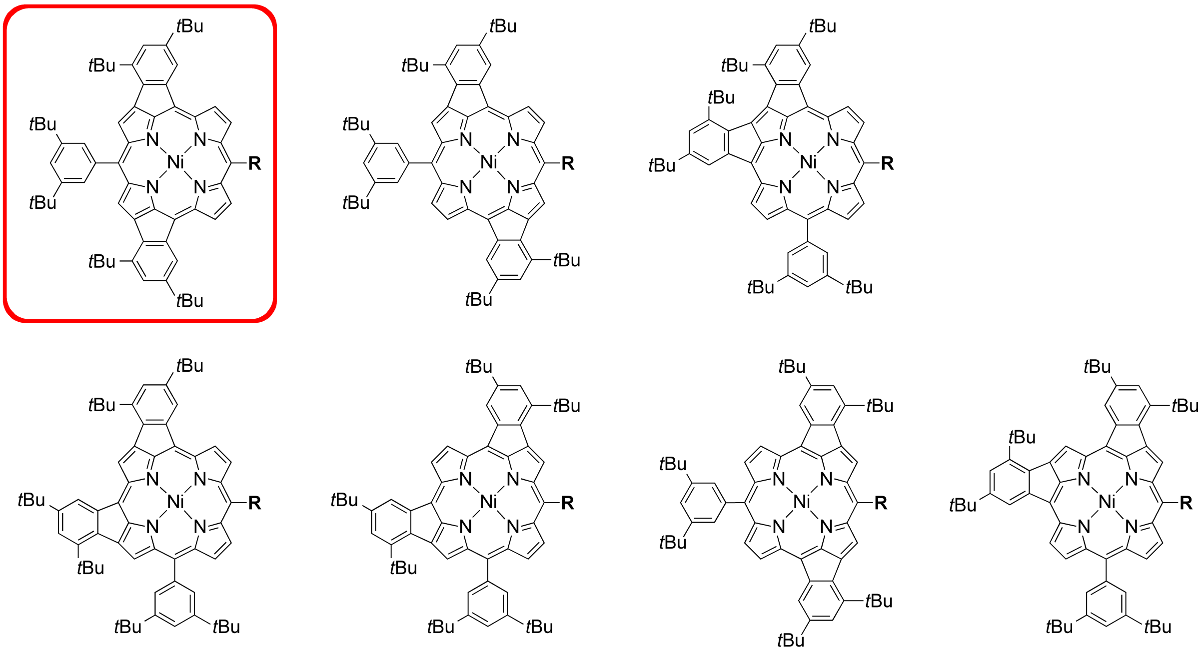

Scheme S 1. Seven different structures as doubly phenylene-fused porphyrins.

2. Instrumentation and Materials

^{1}H NMR (600 MHz) and ^{13}C NMR (151 MHz) spectra were taken on a JEOL ECA-600 spectrometer. Chemical shifts are reported on a delta scale in ppm relative to residual $CHCl_3$ (δ = 7.26 ppm) or 2,3,5,6-tetradeuteriopyridine (δ = 7.58 ppm) for ^{1}H NMR, and to $CDCl_3$ (δ = 77.16 ppm) for ^{13}C NMR. Spectroscopic grade solvents were used for all spectroscopic studies without further purification. UV/Vis/NIR absorption spectra were recorded on a Shimadzu UV-3600PC spectrometer. Atmospheric pressure chemical ionization time-of-flight mass (APCI-TOF-MS) spectra were recorded on a Bruker micrOTOF instrument. Preparative separations were performed by silica gel chromatography (Wako gel C-200, C-300, or C-400) and gel permeation chromatography (Bio-Rad Bio-Beads S-X1, packed with toluene). CH_2Cl_2, $MeNO_2$, and toluene were distilled from CaH_2. THF was purified by passing through a neutral alumina column under N_2. Unless otherwise noted, materials obtained from commercial suppliers were used without further purification.

3. Experimental Procedures and Compound Data

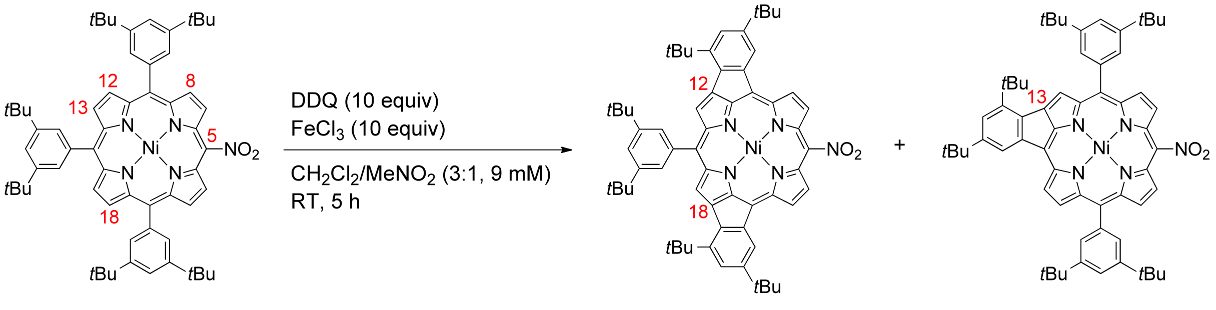

1e **2e**: 29% **3**: 18%

Synthesis of 2e and 3: A flask containing **1e** (17.6 mg, 18 μmol) was purged with argon, and then charged with CH_2Cl_2 (1.5 mL). A solution of $FeCl_3$ (28.4 mg, 180 μmol) and DDQ (40.0 mg, 180 μmol) in $MeNO_2$ (0.5 mL) was added slowly to the mixture. The mixture was stirred at room temperature for 5 h. The reaction was quenched by addition of saturated aqueous $NaHCO_3$ solution. The organic phase was separated and washed with water and brine, and dried over anhydrous Na_2SO_4. After removal of the solvent *in vacuo*, the residue was separated by silica gel chromatography eluting with CH_2Cl_2/hexane. Recrystallization from CH_2Cl_2/methanol gave **2e** (5.0 mg, 5.1 μmol, 29%) and **3** (3.2 mg, 3.3 μmol, 18%).

2e: ^{1}H NMR (600 MHz, $CDCl_3$, 25 °C): δ = 8.91 (d, J = 5.0 Hz, 2H, β), 8.64 (d, J = 5.0 Hz, 2H, β), 7.91 (d, J = 1.4 Hz, 2H, Ar), 7.74 (d, J = 1.8 Hz, 2H, Ar), 7.70 (s, 2H, β), 7.69 (t, J = 1.8 Hz, 1H, Ar), 7.10 (d, J = 1.4 Hz, 2H, Ar), 1.53 (s, 18H, *tert*-butyl), 1.50 (s, 18H, *tert*-butyl), and 1.47 (s, 18H, *tert*-butyl) ppm; ^{13}C NMR (151 MHz, $CDCl_3$, 25 °C): δ = 155.78, 152.35, 149.96, 148.08, 147.56, 147.12, 145.76, 141.64, 141.36, 136.54, 133.21, 130.75, 130.34, 130.13, 129.38, 128.95, 127.59, 124.19, 121.98, 121.03, 118.68, 35.42, 35.24, 35.14, 31.79, 31.31, and 29.18 ppm; APCI-TOF-MS: *m*/*z* = 971.4658. Calcd for $C_{62}H_{67}O_2N_5{}^{58}Ni$: 971.4654 $[M]^-$; UV/Vis (CH_2Cl_2): λ_{max} (ε [$M^{-1}cm^{-1}$]) = 441 (7.81 × 10^4), 521 (4.18 × 10^4), 624 (5.79 × 10^3), 732 (3.42 × 10^3), and 814 nm (1.91 × 10^3).

3: ^{1}H NMR (600 MHz, $CDCl_3$, 25 °C): δ = 9.10 (d, J = 5.0 Hz, 1H, β), 8.78 (d, J = 5.0 Hz, 1H, β), 8.76 (d, J = 5.0 Hz, 1H, β), 8.64 (d, J = 5.0 Hz, 1H, β), 8.58 (d, J = 5.0 Hz, 1H, β), 8.48 (d, J = 5.0 Hz, 1H, β), 7.95-7.93 (m, 2H, Ar + β), 7.79 (d, J = 1.9 Hz, 2H, Ar), 7.76 (d, J = 1.9 Hz, 2H, Ar), 7.75-7.72 (m, 2H, Ar), 7.04 (s, 1H, Ar), 1.54 (s, 9H, *tert*-butyl), 1.50 (s, 18H, *tert*-butyl), 1.49 (s, 18H, *tert*-butyl), and 1.46 (s, 9H, *tert*-butyl) ppm; ^{13}C NMR (151 MHz, $CDCl_3$, 25 °C): δ = 154.74, 153.07, 150.24, 149.72, 149.48, 148.99, 147.89, 147.69, 146.55, 146.23, 145.23, 140.90, 139.33, 138.11, 137.89, 137.54, 135.64, 134.43, 133.49 (overlap), 131.19, 129.35, 128.71, 128.61, 128.22, 127.43, 126.46, 125.99, 123.87, 122.57, 121.72 (overlap), 121.35, 116.54, 35.43, 35.23, 35.17 (overlap), 31.81, 31.21, 29.87, and 29.13 ppm; APCI-TOF-MS: *m*/*z* = 973.4828. Calcd for $C_{62}H_{69}N_5{}^{58}NiO_2$: 973.4810 $[M]^-$; UV/Vis (CH_2Cl_2): λ_{max} (ε [$M^{-1}cm^{-1}$]) = 439 (6.64 × 10^4), 473 (5.23 × 10^4), 575 (5.65 × 10^3), 622 (4.98 × 10^3), and 669 nm (3.66 × 10^3).

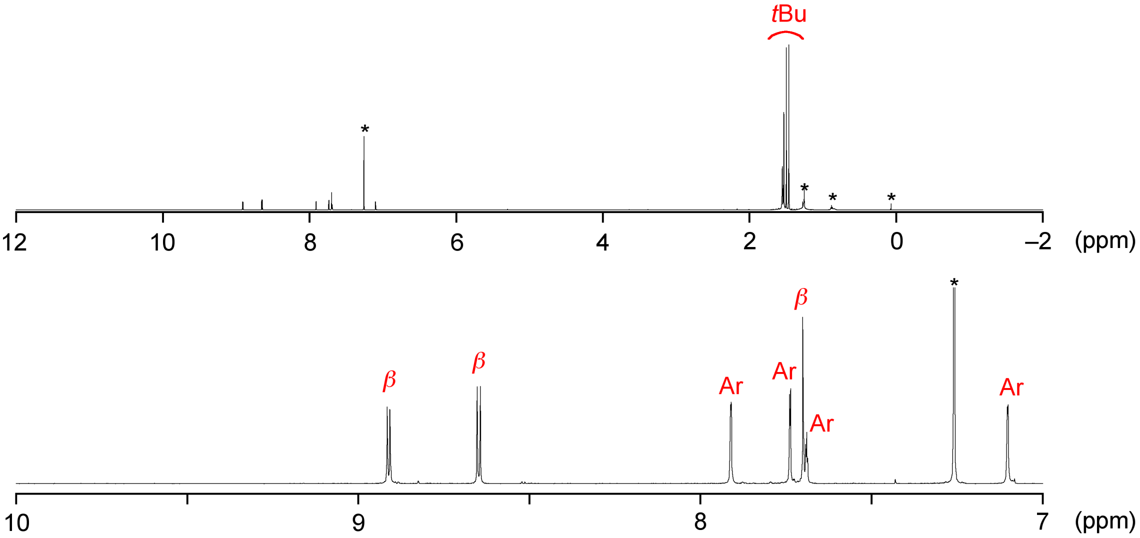

Figure S 1. ^{1}H NMR spectrum of **2e** in CDCl$_3$ at 25 °C. *Solvent and impurities.

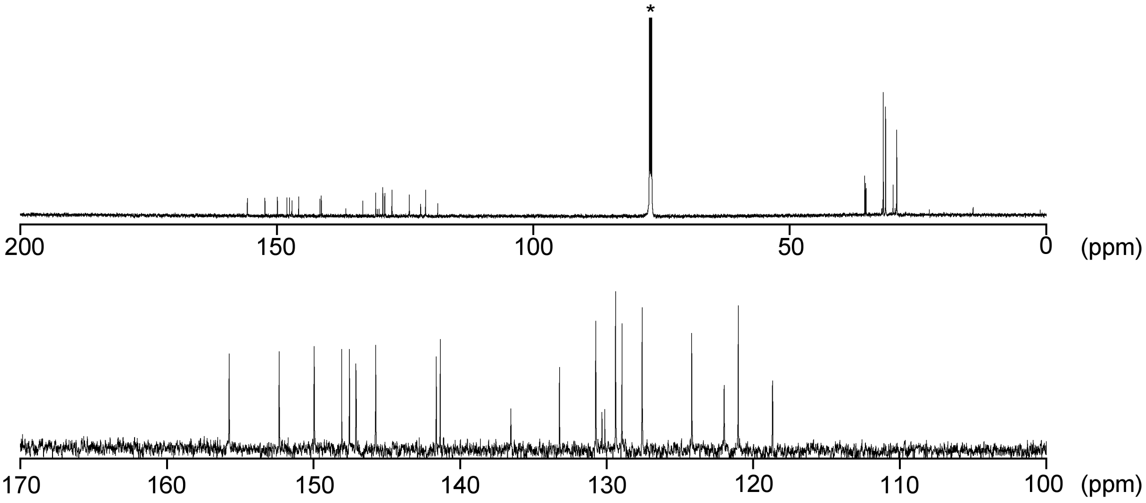

Figure S 2. ^{13}C NMR spectrum of **2e** in CDCl$_3$ at 25 °C. *Solvent.

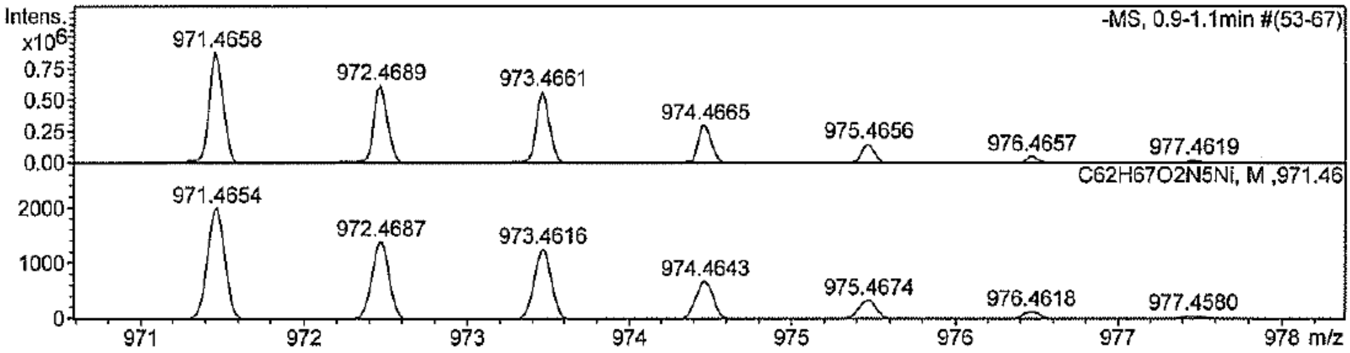

Figure S 3. Observed (top) and simulated (bottom) HR-APCI-TOF MS of **2e**.

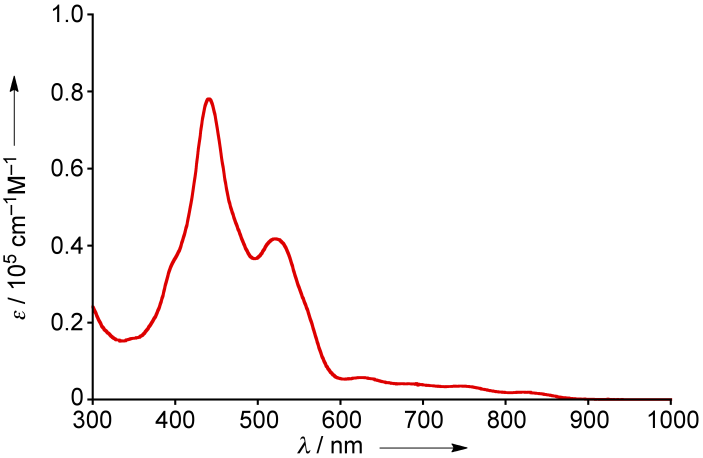

Figure S 4. UV / Vis absorption spectrum of **2e** in CH$_2$Cl$_2$.

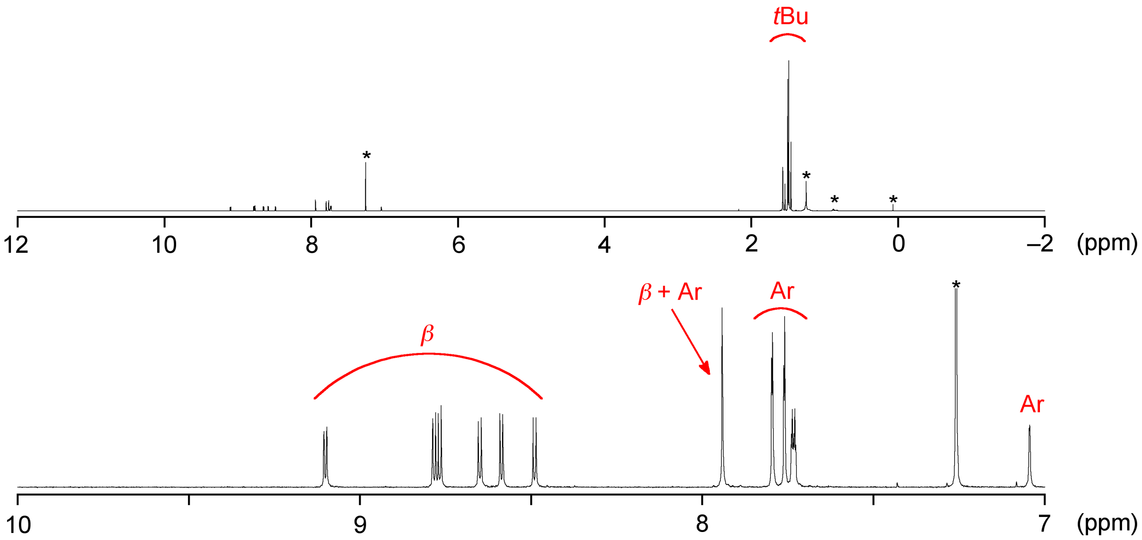

Figure S 5. ^{1}H NMR spectrum of **3** in CDCl$_3$ at 25 °C. *Solvent and impurities.

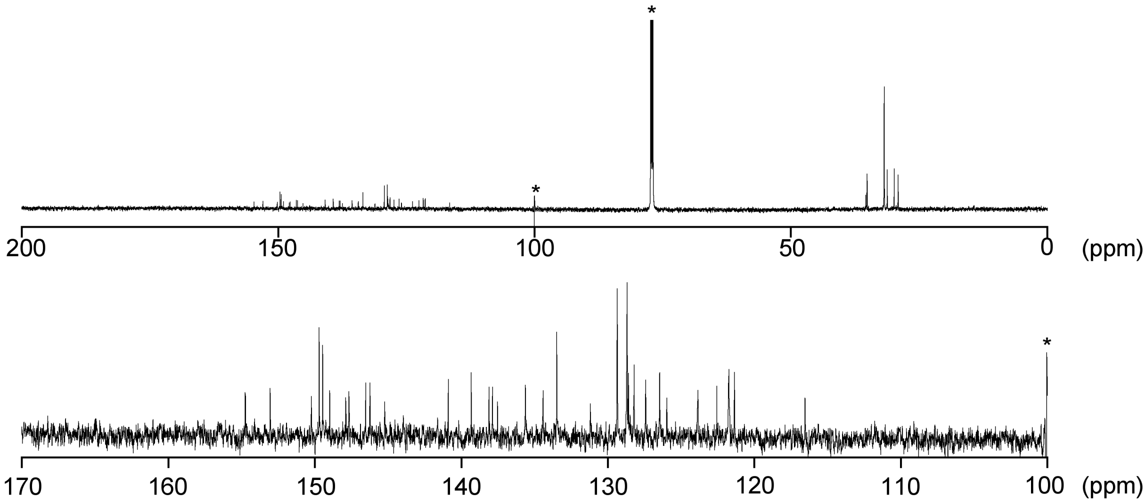

Figure S 6. ^{13}C NMR spectrum of **3** in CDCl$_3$ at 25 °C. *Solvent and impurity.

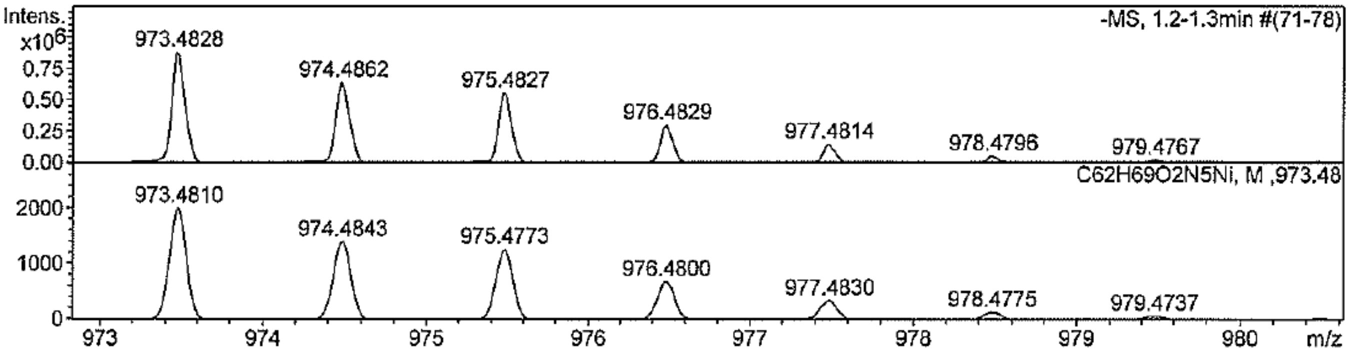

Figure S 7. Observed (top) and simulated (bottom) HR-APCI-TOF MS of **3**.

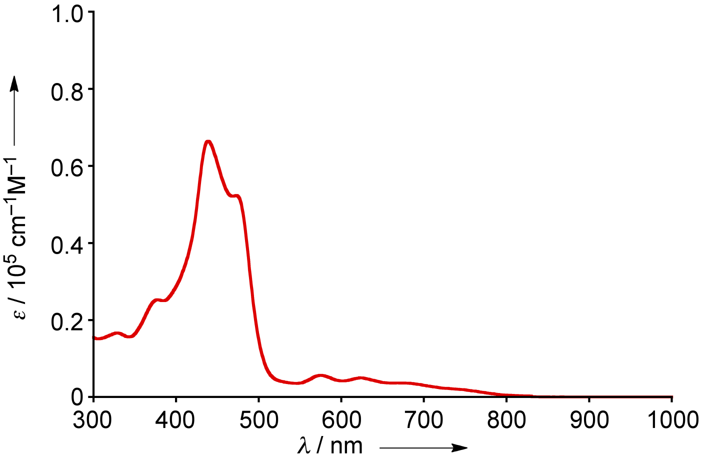

Figure S 8. UV/Vis absorption spectrum of **3** in CH_2Cl_2.

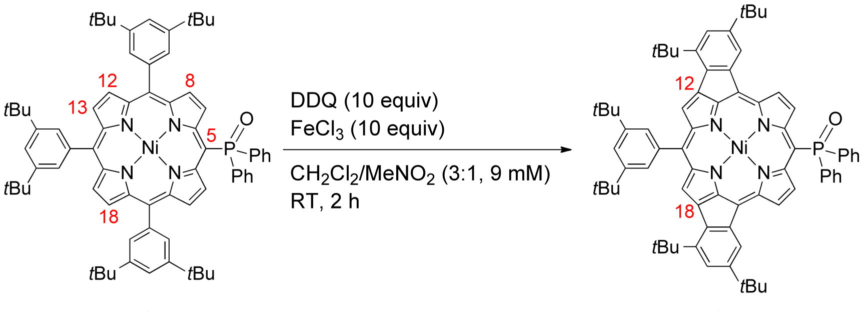

Synthesis of 2f: A flask containing **1f** (20.0 mg, 18 μmol) was purged with argon, and then charged with CH_2Cl_2 (1.5 mL). A solution of $FeCl_3$ (28.4 mg, 180 μmol) and DDQ (40.0 mg, 180 μmol) in $MeNO_2$ (0.5 mL) was added slowly to the mixture. The mixture was stirred at room temperature for 2 h. The reaction was quenched by addition of saturated aqueous $NaHCO_3$ solution. The organic phase was separated and washed with water and brine, and dried over anhydrous Na_2SO_4. After removal of the solvent *in vacuo*, the residue was separated by silica gel chromatography eluting with CH_2Cl_2/hexane. Recrystallization from CH_2Cl_2/methanol gave **2f** (12.2 mg, 10.8 μmol, 61%).

2f: ^{1}H NMR (600 MHz, $CDCl_3$, 25 °C): $\delta = 8.69$ (d, $J = 5.0$ Hz, 2H, β), 8.54 (d, $J = 5.0$ Hz, 2H, β), 7.79 (d, $J = 1.9$ Hz, 2H, Ar), 7.75 (d, $J = 1.9$ Hz, 2H, Ar), 7.73-7.65 (m, 7H, β + Ar + Ph), 7.48 (t, $J = 7.8$ Hz, 2H, Ph), 7.38 (t, $J = 7.8$ Hz, 4H, Ph), 7.08 (s, 2H, Ar), 1.53 (s, 18H, *tert*-butyl), 1.49 (s, 18H, *tert*-butyl), and 1.41 (s, 18H, *tert*-butyl) ppm; ^{13}C NMR (151 MHz, $CDCl_3$, 25 °C): δ = 155.21, 151.82, 149.99, 149.70 (d, *J* = 14.4 Hz), 148.06, 146.75, 146.34, 144.55, 139.69, 137.96 (d, *J* = 105.5 Hz), 136.58, 135.21, 133.47, 131.80 (d, *J* = 8.7 Hz), 131.54, 130.52, 129.15, 128.79 (d, *J* = 11.6 Hz), 128.25, 127.27, 123.80, 121.84, 120.82, 117.39, 103.46 (d, *J* = 111.3 Hz), 35.41, 35.17, 35.12, 31.77, 31.30, and 29.15 ppm; APCI-TOF-MS: *m*/*z* = 1126.5180. Calcd for $C_{74}H_{77}N_4{}^{58}NiOP$: 1126.5194 $[M]^-$; UV/vis (CH_2Cl_2): λ_{max} (ε [$M^{-1}cm^{-1}$]) = 402 (4.44 × 10^4), 448 (7.02 × 10^4), 515 (3.92 × 10^4), 540 (3.76 × 10^4), 630 (5.65 × 10^3), 730 (3.90 × 10^3), and 818 nm (2.20 × 10^3).

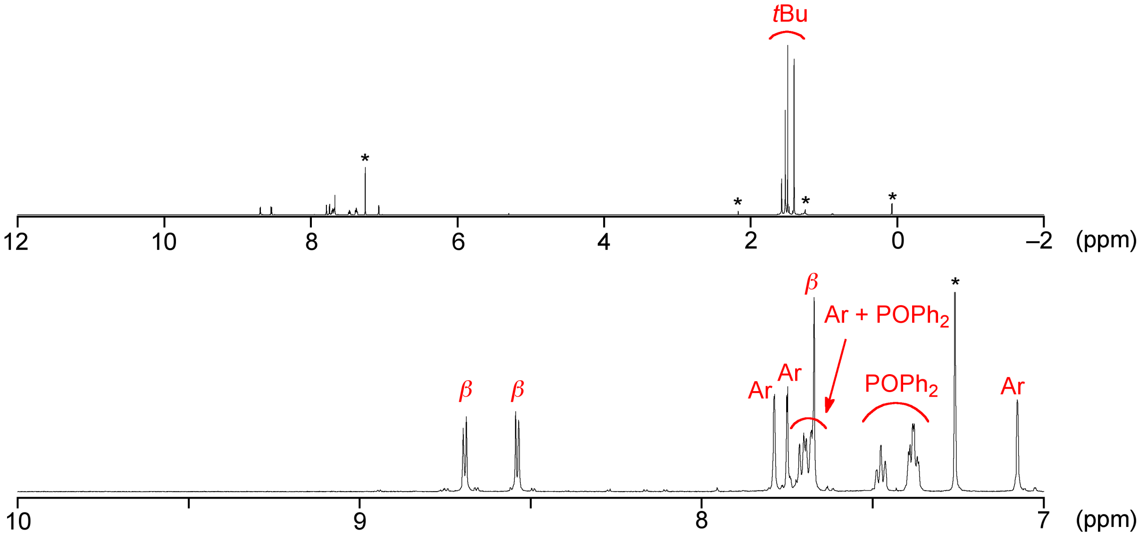

Figure S 9. ^{1}H NMR spectrum of **2f** in $CDCl_3$ at 25 °C. *Solvent and impurities.

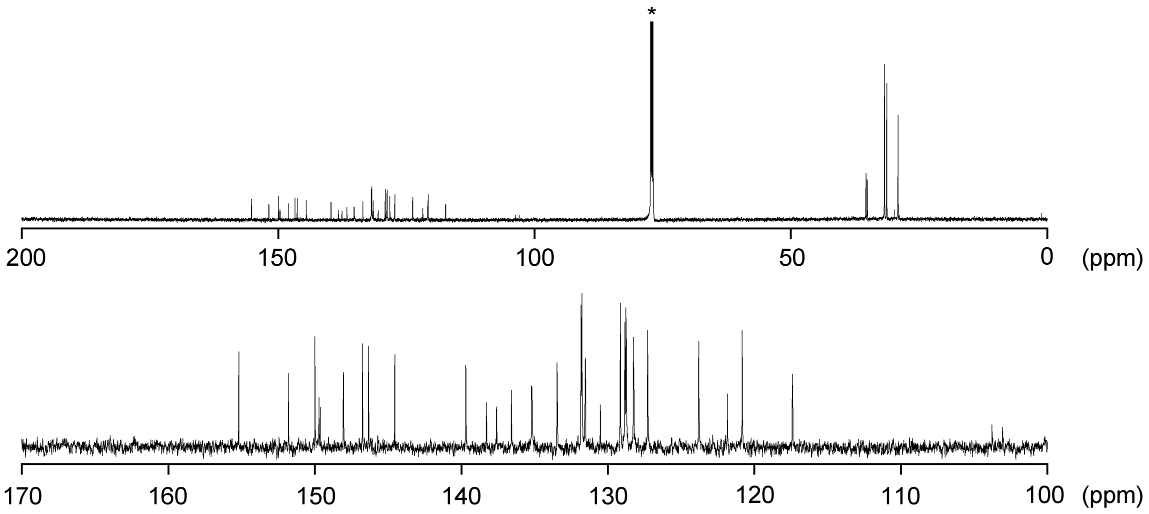

Figure S 10. ^{13}C NMR spectrum of **2f** in $CDCl_3$ at 25 °C. *Solvent.

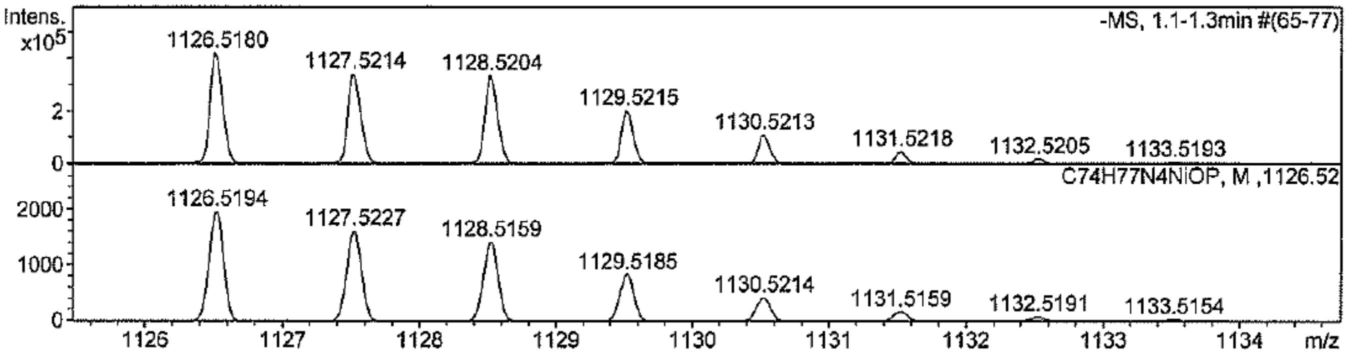

Figure S 11. Observed (top) and simulated (bottom) HR-APCI-TOF MS of **2f**.

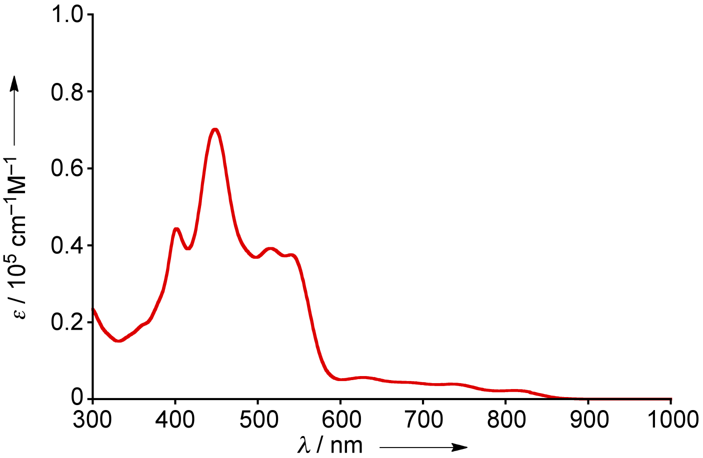

Figure S 12. UV/Vis absorption spectrum of **2f** in CH_2Cl_2.

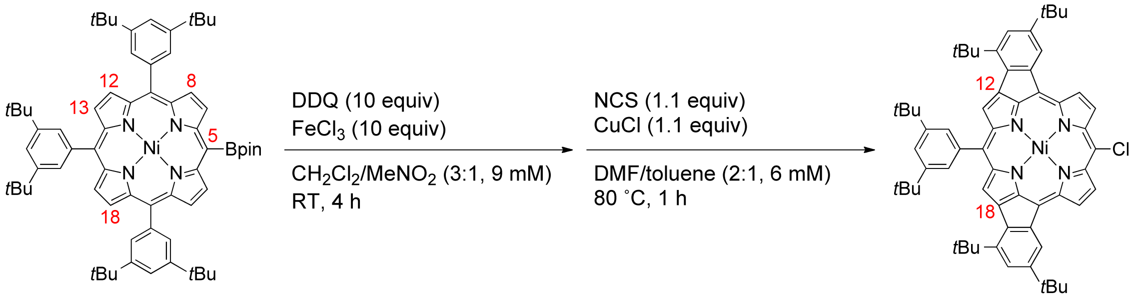

1g

2c: 37%

Synthesis of 2c: A flask containing **1g** (19.0 mg, 18 μmol) was purged with argon, and then charged with CH_2Cl_2 (1.5 mL). A solution of $FeCl_3$ (28.4 mg, 180 μmol) and DDQ (40 mg, 180 μmol) in $MeNO_2$ (0.5 mL) was added slowly to the mixture. The mixture was stirred at room temperature for 4 h. The reaction was quenched by addition of saturated aqueous $NaHCO_3$ solution. The organic phase was separated and washed with water and brine, and dried over anhydrous Na_2SO_4. After removal of the solvent *in vacuo*, the residue was charged with *N*-chlorosuccinimide (2.7 mg, 20 μmol), CuCl (2.0 mg, 20 μmol), DMF (2.0 mL), and toluene (1.0 mL). The mixture was stirred at 80 ˚C for 1 h. The reaction was quenched with a sufficient amount of aqueous $Na_2S_2O_3$ solution, extracted with CH_2Cl_2, washed with H_2O twice and brine, and dried over anhydrous Na_2SO_4. After removal of the solvent *in vacuo*, the residue was separated by silica gel chromatography eluting with CH_2Cl_2/hexane. Recrystallization from CH_2Cl_2/methanol gave **2c** (6.4 mg, 6.7 μmol, 37%).

2c: ^{1}H NMR (600 MHz, CDCl$_3$, 25 °C): δ = 9.01 (d, J = 5.0 Hz, 2H, β), 8.83 (d, J = 5.0 Hz, 2H, β), 7.90 (d, J = 1.8 Hz, 2H, Ar), 7.77 (d, J = 1.8 Hz, 2H, Ar), 7.73 (s, 2H, β), 7.68 (t, J = 1.8 Hz, 1H, Ar), 7.06 (d, J = 1.8 Hz, 2H, Ar), 1.55 (s, 18H, *tert*-butyl), 1.51 (s, 18H, *tert*-butyl), and 1.47 (s, 18H, *tert*-butyl) ppm; ^{13}C NMR (151 MHz, CDCl$_3$, 25 °C): δ = 154.59, 152.00, 149.76, 148.90, 147.75, 146.83, 145.73, 145.33, 141.47, 136.94, 133.14, 132.59, 129.55 (overlap), 128.01, 127.52, 127.15, 123.41, 121.62, 120.71, 116.62, 35.41, 35.20, 35.12, 31.81, 31.34, and 29.23 ppm; APCI-TOF-MS: *m*/*z* = 960.4414. Calcd for $C_{62}H_{67}{}^{35}ClN_4{}^{58}Ni$: 960.4413 $[M]^{-}$; UV/Vis (CH$_2$Cl$_2$): λ_{max} (ε [M^{-1}cm^{-1}]) = 399 (3.66 × 10^4), 438 (5.07 × 10^4), 510 (4.62 × 10^4), 688 (4.95 × 10^3), 741 (3.50 × 10^3), and 825 nm (1.66 × 10^3).

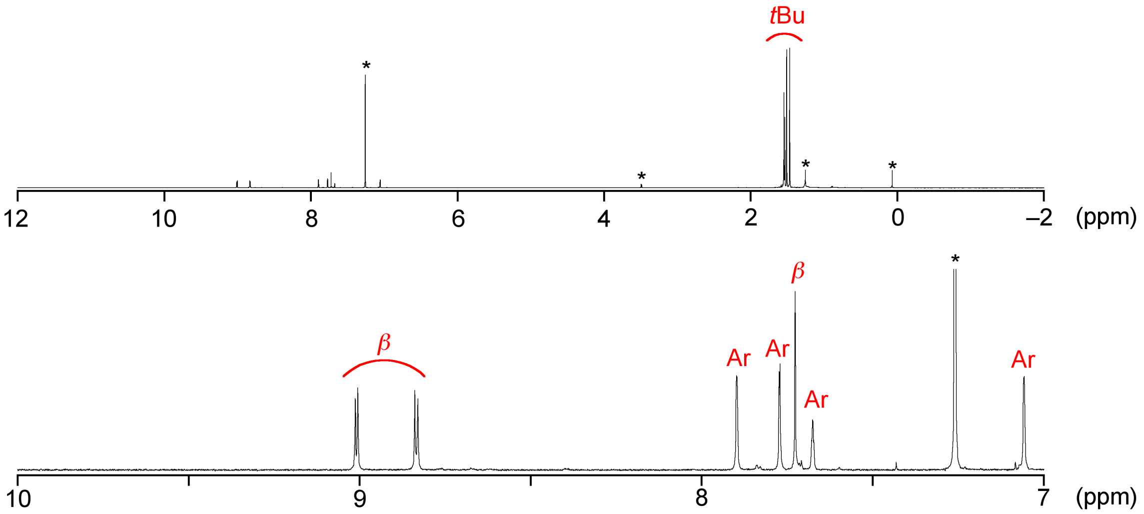

Figure S 13. ^{1}H NMR spectrum of **2c** in CDCl$_3$ at 25 °C. *Solvent and impurities.

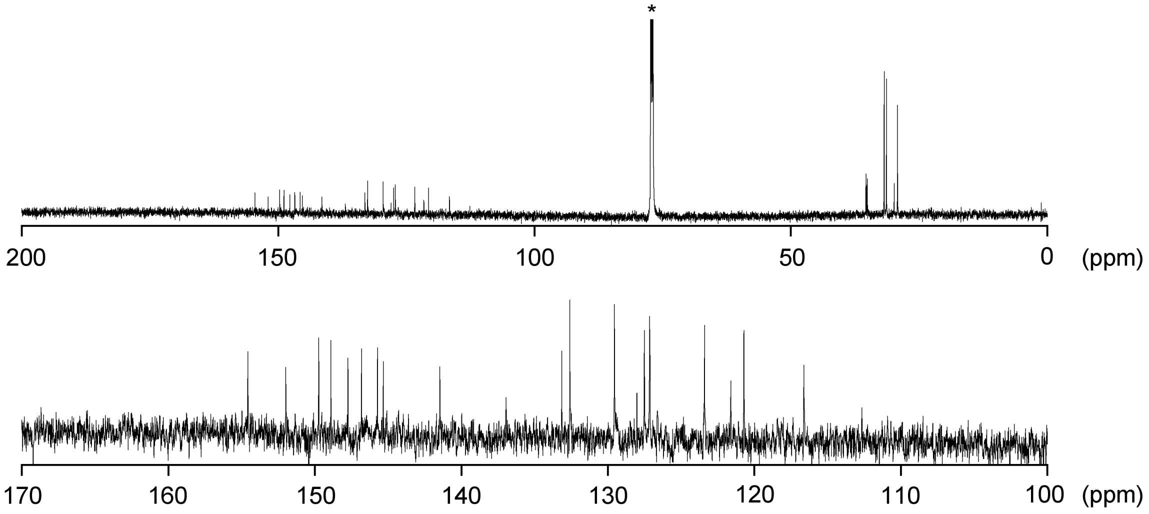

Figure S 14. ^{13}C NMR spectrum of **2c** in CDCl$_3$ at 25 °C. *Solvent.

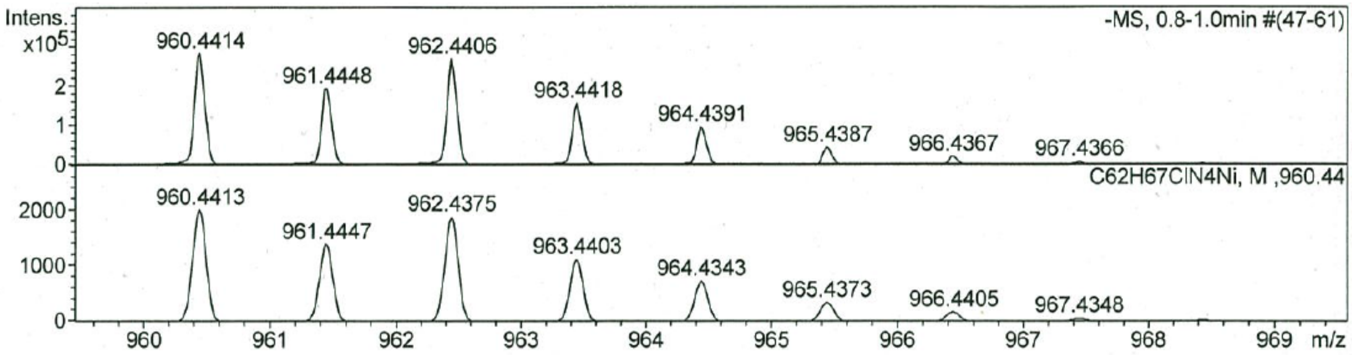

Figure S 15. Observed (top) and simulated (bottom) HR-APCI-TOF MS of **2c**.

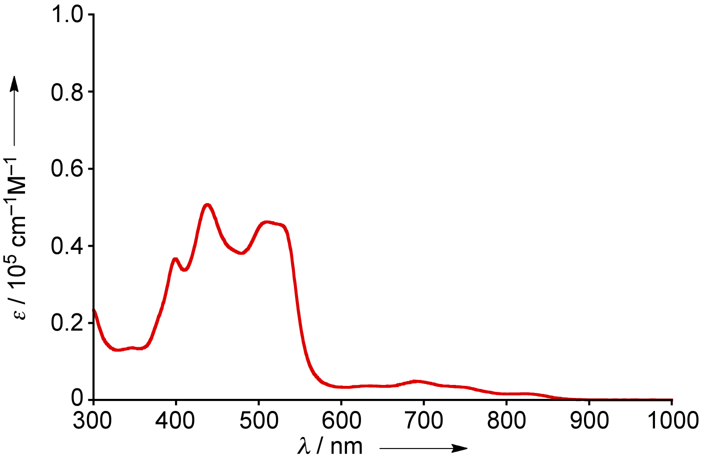

Figure S 16. UV/Vis absorption spectrum of **2c** in CH_2Cl_2.

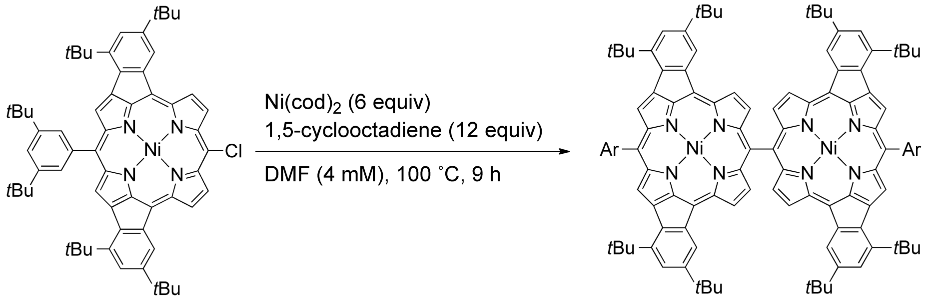

2c

5Ni: 83%

Synthesis of 5Ni: A flask containing **2c** (22.5 mg, 23 μmol) and Ni(cod)$_2$ (38.6 mg, 138 μmol) was purged with argon, and then charged with DMF (8.0 mL) and 1,5-cyclooctadiene (34 μL, 138 μmol). The mixture was stirred at 100 ˚C for 9 h. The reaction mixture was diluted with CH_2Cl_2, washed with H_2O twice and then with brine, and dried over anhydrous Na_2SO_4. After removal of the solvent *in vacuo*, the residue was separated by silica gel chromatography eluting with CH_2Cl_2/hexane and gel permeation chromatography (GPC) eluting with toluene. Recrystallization from CH_2Cl_2/methanol gave **5Ni** (18.0 mg, 9.7 μmol, 83%).

5Ni: ^{1}H NMR (600 MHz, $CDCl_3$, 25 °C): δ = 8.68 (d, J = 5.0 Hz, 4H, β), 7.88-7.84 (m, 12H, Ar + β), 7.73-7.70 (m, 6H, Ar + β), 7.06 (s, 4H, Ar), 1.65 (s, 36H, *tert*-butyl), 1.55 (s, 36H, *tert*-butyl), and 1.37 (s, 36H, *tert*-butyl) ppm; ^{13}C NMR (151 MHz, $CDCl_3$, 25 °C): δ = 154.99, 151.86, 150.48, 149.78, 148.97, 147.23, 146.69, 145.29, 141.33, 137.16, 135.80, 133.80, 129.64, 128.51, 127.08 (overlap), 123.26, 121.63, 120.71, 117.05, 116.34, 35.46, 35.17, 35.14, 31.25, 29.86, and

29.28 ppm; APCI-TOF-MS: m/z = 1850.9366. Calcd for $C_{124}H_{134}N_8{}^{58}Ni_2$: 1850.9444 $[M]^-$; UV/Vis (CH_2Cl_2): λ_{max} (ε [$M^{-1}cm^{-1}$]) = 437 (1.39×10^5), 512 (1.44×10^5), 694 (1.43×10^4), 750 (1.51×10^4), and 824 nm (1.24×10^4).

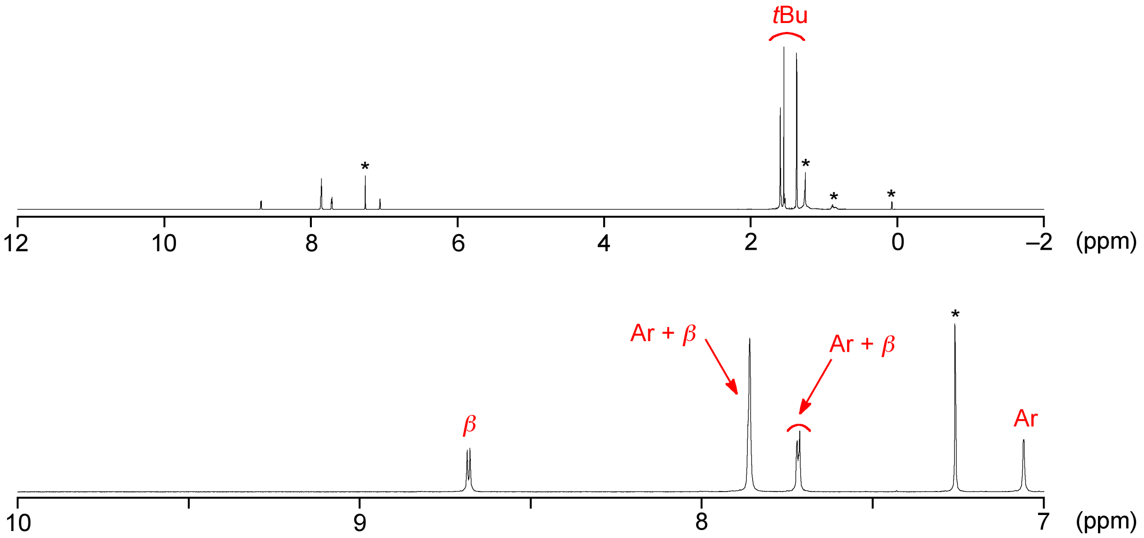

Figure S 17. ^{1}H NMR spectrum of **5Ni** in $CDCl_3$ at 25 °C. *Solvent and impurities.

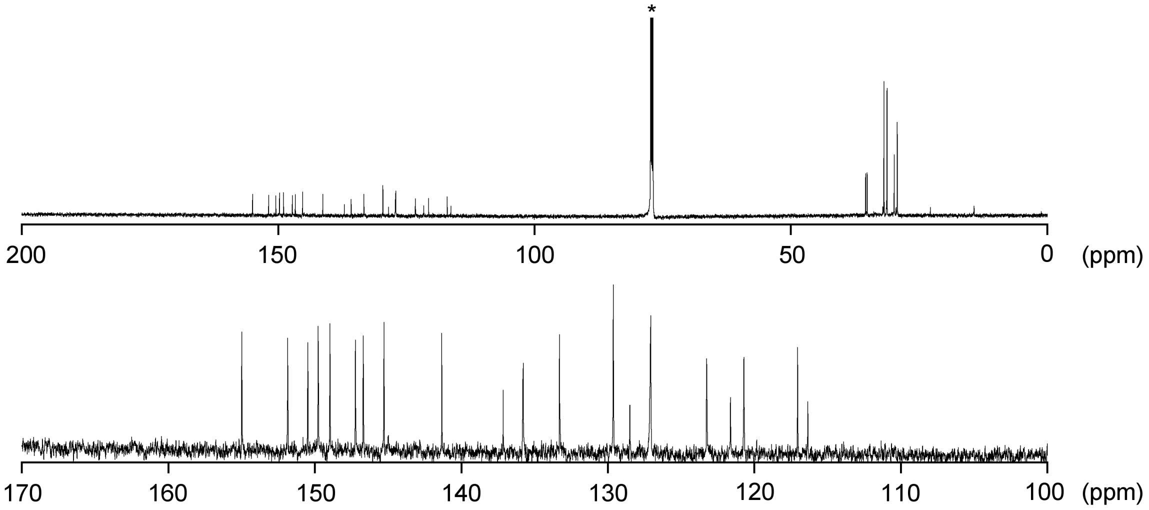

Figure S 18. ^{13}C NMR spectrum of **5Ni** in $CDCl_3$ at 25 °C. *Solvent.

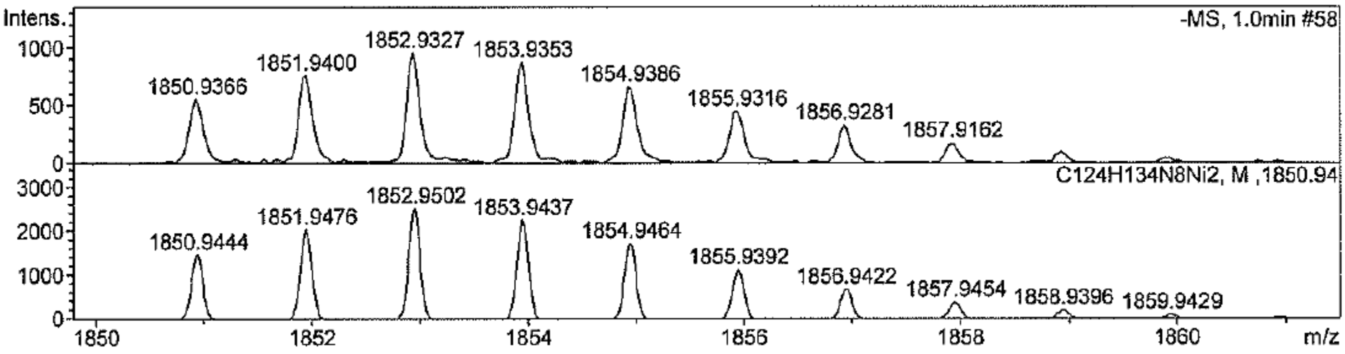

Figure S 19. Observed (top) and simulated (bottom) HR-APCI-TOF MS of **5Ni**.

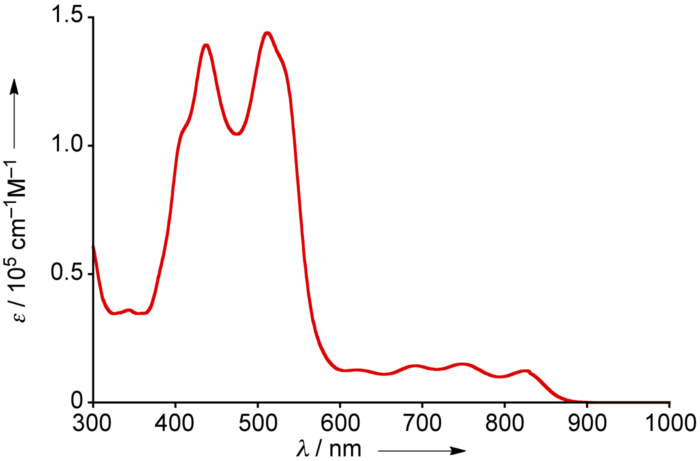

Figure S 20. UV/Vis absorption spectrum of **5Ni** in CH_2Cl_2.

5Ni

5Zn: 85%

Synthesis of 5Zn: Conc. H_2SO_4 (0.8 mL) was added slowly to a mixture of **5Ni** (11.2 mg, 6.0 μmol) and TFA (3.2 mL) at 0 °C. The reaction mixture was stirred at 0 °C in air for 30 min, and then poured into water at 0 °C. After neutralization by NaOH and K_2CO_3 at 0 °C, the product was extracted with CH_2Cl_2, washed with brine, and dried over anhydrous Na_2SO_4. After removal of the solvent *in vacuo*, the residue was dissolved in CH_2Cl_2, and charged with an excess amount of $Zn(OAc)_2 \cdot 2H_2O$ dissolved in MeOH. The mixture was stirred for 1 h at room temperature. After removal of the solvent *in vacuo*, the residue was separated by silica gel chromatography eluting with CH_2Cl_2/hexane. Recrystallization from CH_2Cl_2/methanol gave **5Zn** (9.6 mg, 5.2 μmol, 85%).

5Zn: ^{1}H NMR of **5Zn** with 2 equivalents of pyridine (600 MHz, $CDCl_3$, 25 °C): δ = 8.57 (d, J = 5.0 Hz, 4H, β), 7.93 (d, J = 1.9 Hz, 4H, Ar), 7.91 (d, J = 1.9 Hz, 4H, Ar), 7.72 (s, 4H, β), 7.70 (t, J = 1.9 Hz, 2H, Ar), 7.40 (d, J = 5.0 Hz, 4H, β), 7.12 (t, J = 7.8 Hz, 2H, pyridine), 6.98 (s, 4H, Ar), 6.50 (t, J = 7.8 Hz, 4H, pyridine), 5.25 (br-s, 4H, pyridine), 1.63 (s, 36H, *tert*-butyl), 1.57 (s, 36H, *tert*-butyl), and 1.38 (s, 36H, *tert*-butyl) ppm; ^{13}C NMR of **5Zn** with 2 equivalents of pyridine (151 MHz, $CDCl_3$, 25 °C): δ = 162.23, 156.05, 155.20, 151.78, 151.51, 149.28, 147.13, 146.56, 145.79, 145.28, 138.89, 137.00, 135.15, 134.61, 130.84, 130.55, 126.90, 126.20, 123.70, 122.61, 120.96, 120.58, 118.25, 117.28, 35.46, 35.14, 35.05, 31.93, 31.24, and 29.33 ppm; APCI-TOF-MS: m/z = 1862.9249. Calcd for $C_{124}H_{134}N_8{}^{64}Zn_2$: 1862.9320 $[M]^{-}$; UV/Vis (CH_2Cl_2): λ_{max} (ε [$M^{-1}cm^{-1}$]) = 426 (9.51×10^4), 487 (1.30×10^5), 780 (1.54×10^4), and 836 nm (1.05×10^4); UV/Vis (CH_2Cl_2 + pyridine 1%): λ_{max} (ε [$M^{-1}cm^{-1}$]) = 430 (8.11×10^4), 487 (1.14×10^5), 534 (1.01×10^5), 616 (3.31×10^4), 789 (1.67×10^4), and 855 nm (1.26×10^4).

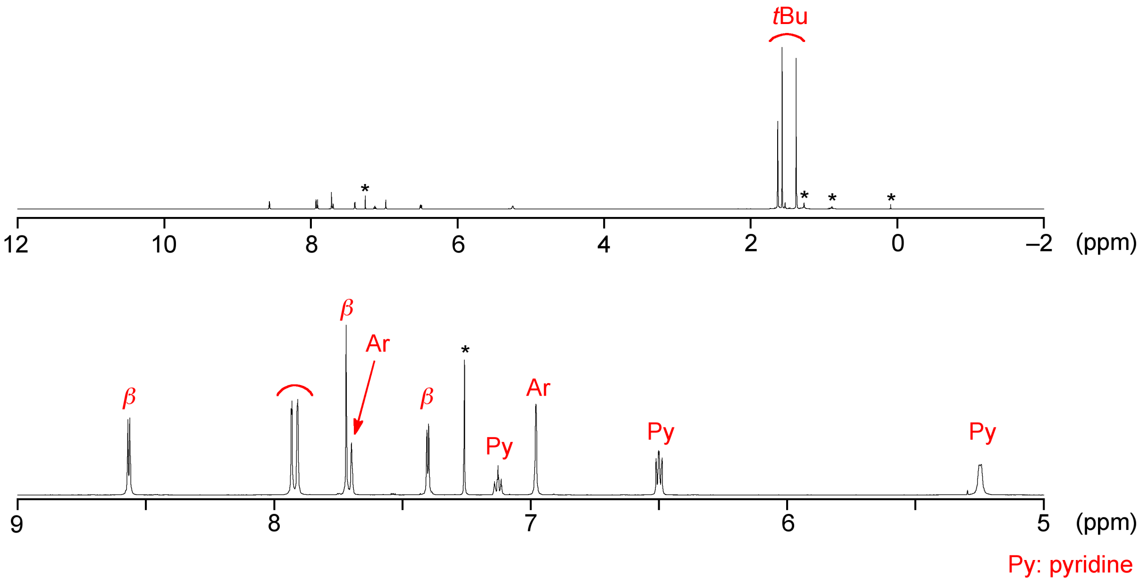

Figure S 21. ^{1}H NMR spectrum of **5Zn** in CDCl$_3$ at 25 °C. *Solvent and impurities.

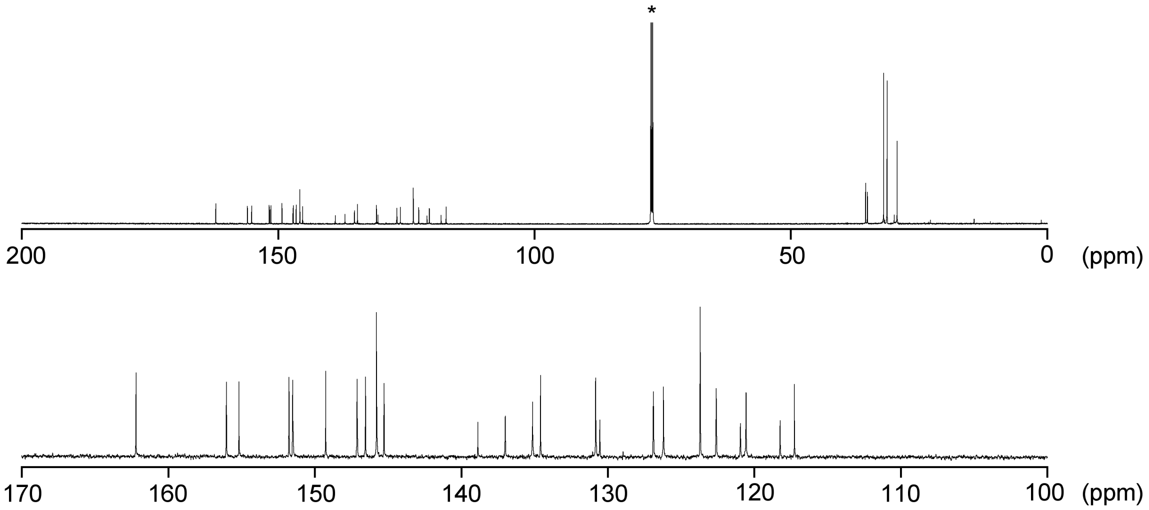

Figure S 22. ^{13}C NMR spectrum of **5Zn** in CDCl$_3$ at 25 °C. *Solvent.

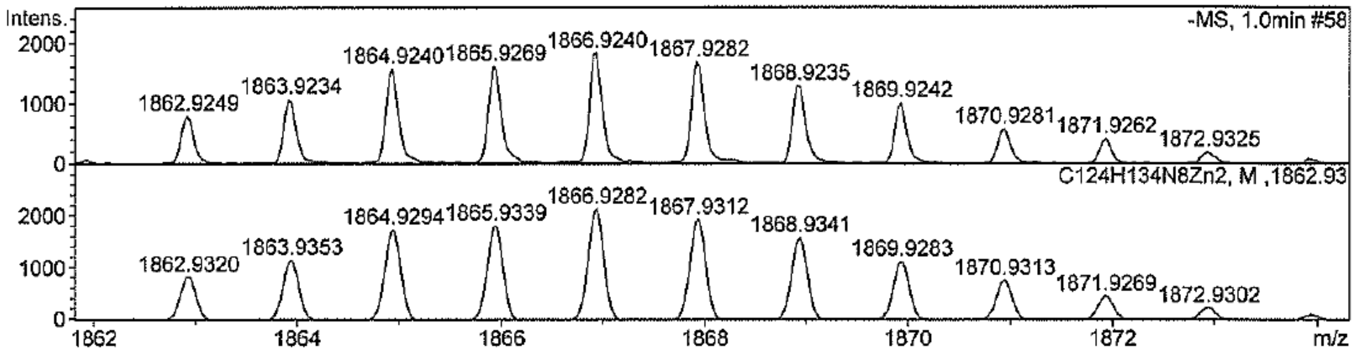

Figure S 23. Observed (top) and simulated (bottom) HR-APCI-TOF MS of **5Zn**.

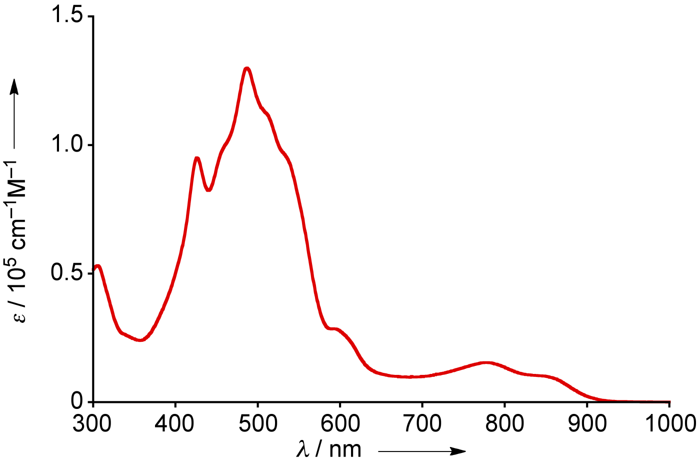

Figure S 24. UV/Vis absorption spectrum of **5Zn** in CH_2Cl_2.

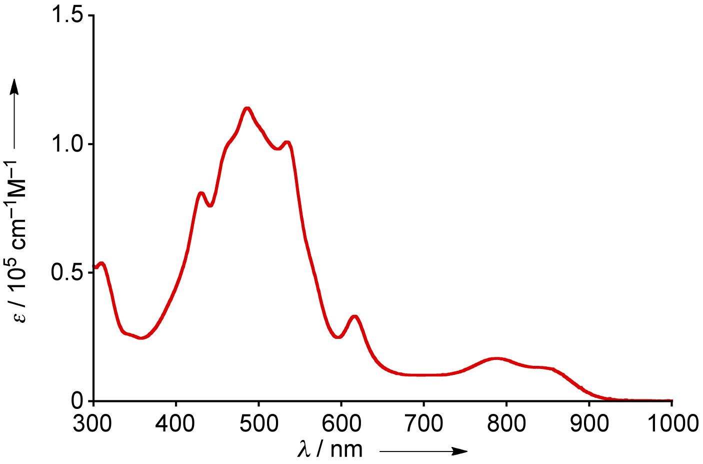

Figure S 25. UV/Vis absorption spectrum of **5Zn** in CH_2Cl_2 containing 1% of pyridine.

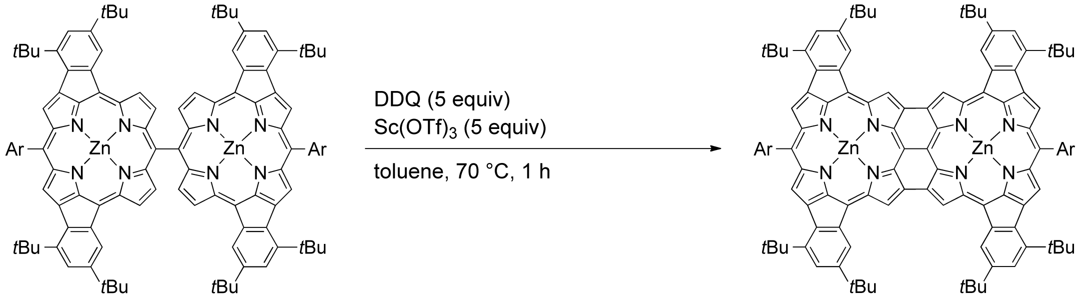

5Zn

6: 60%

Synthesis of 6: A flask containing **5Zn** (11.2 mg, 6.0 μmol), DDQ (6.8 mg, 30 μmol), and $Sc(OTf)_3$ (14.8 mg, 30 μmol) was purged with argon, and then charged with toluene (3.0 mL). The mixture was stirred at 70 °C for 1 h. The reaction mixture was filtered through a small plug of alumina with copious washings (THF). After removal of the solvent *in vacuo*, the residue was separated by silica gel chromatography eluting with CH_2Cl_2/hexane/pyridine. Recrystallization from CH_2Cl_2/methanol gave **6** (6.7 mg, 3.6 μmol, 60%).

6: ^1H NMR (600 MHz, pyridine-d_5, 25 °C): $\delta = 8.19$ (s, 4H), 8.06 (s, 4H), 8.00 (d, $J = 1.9$ Hz, 4H), 7.86 (t, $J = 1.9$ Hz, 2H), 7.33 (s, 4H), 7.29 (s, 4H), 1.57 (s, 36H), 1.47 (s, 36H), and 1.46 (s, 36H) ppm; (The signals for the carbons of **6** are unobservable because of the low solubility.); APCI-TOF-MS: *m*/*z* = 1858.8967. Calcd for $C_{124}H_{130}N_8{}^{64}Zn_2$: 1858.9007 $[M]^-$;

UV/Vis/NIR (CH_2Cl_2 + pyridine 1%): λ_{max} (ε [$M^{-1}cm^{-1}$]) = 476 (1.02×10^5), 565 (4.11×10^4), 611 (3.73×10^4), 661 (2.58×10^4), 851 (4.42×10^4), and 1358 nm (1.88×10^4).

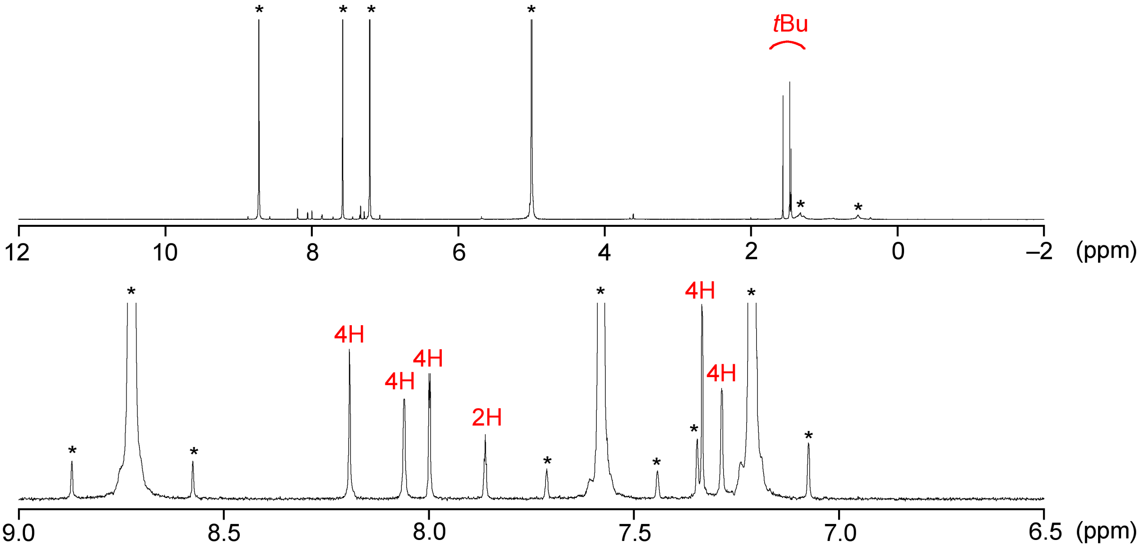

Figure S 26. ^1H NMR spectrum of **6** in pyridine-d_5 at 25 °C. *Solvent and impurities.

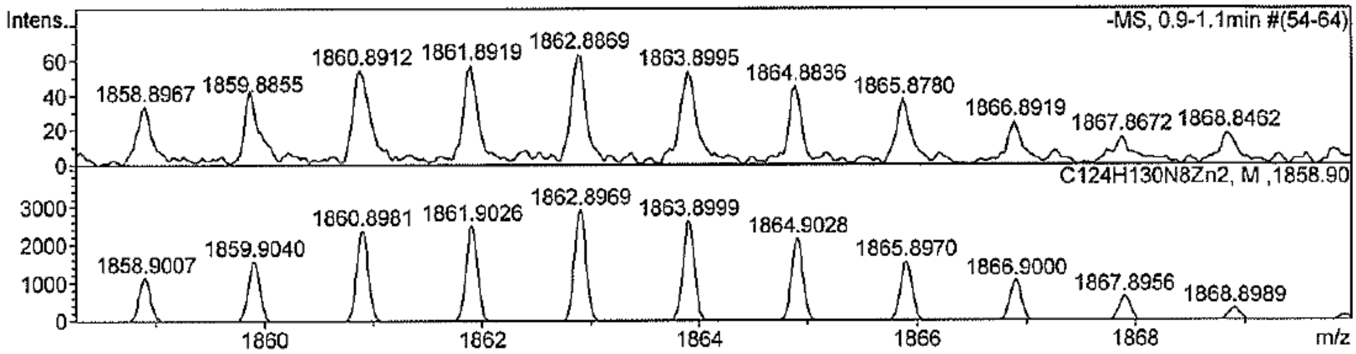

Figure S 27. Observed (top) and simulated (bottom) HR-APCI-TOF MS of **6**.

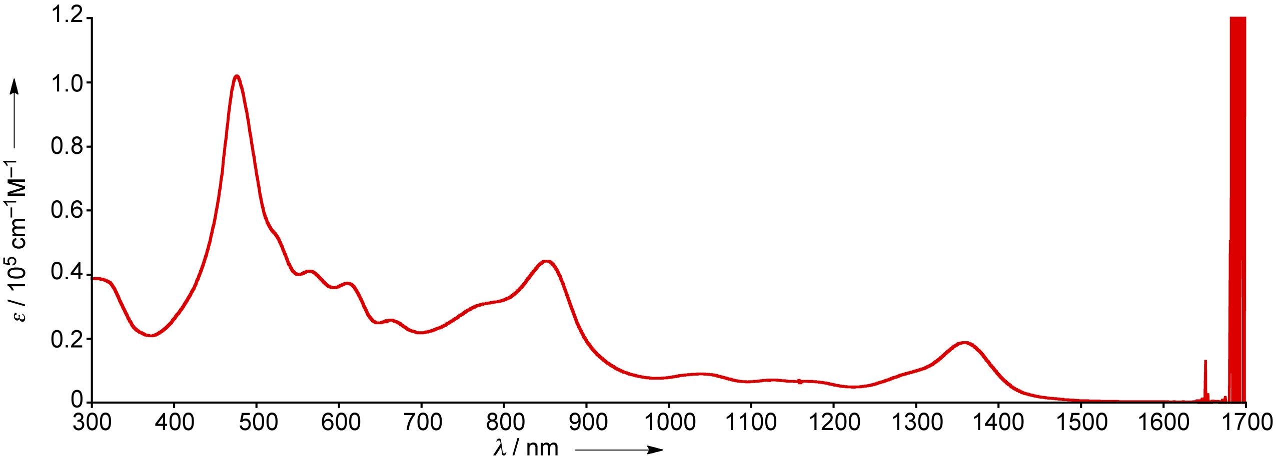

Figure S 28. UV/Vis absorption spectrum of **6** in CH_2Cl_2 containing 1% of pyridine.

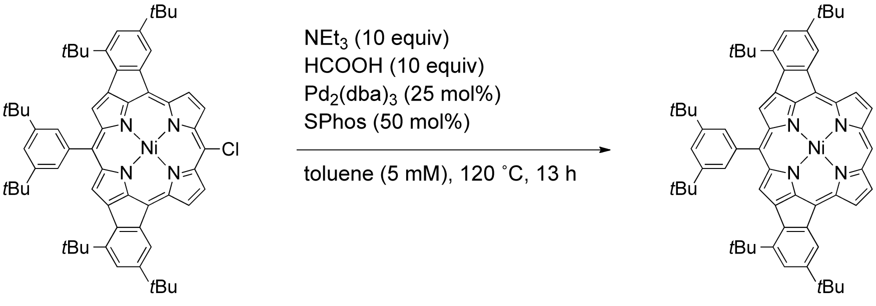

2c

8Ni: 87%

Synthesis of 8Ni: A flask containing **2c** (9.6 mg, 10 μmol), $Pd_2(dba)_3$ (2.3 mg, 2.5 μmol), and Sphos (2.1 mg, 5.0 μmol) was purged with argon, and then charged with toluene (2.0 mL), NEt_3 (14 μL, 0.1 mmol), and HCOOH (4 μL, 0.1 mmol). The mixture was stirred at 120 ˚C for 13 h. The reaction mixture was diluted with CH_2Cl_2 and filtered through a small plug of silica gel with copious washings (CH_2Cl_2). After removal of the solvent *in vacuo*, the residue was separated by silica gel chromatography eluting with CH_2Cl_2/hexane to afford **8Ni**. Recrystallization from CH_2Cl_2/methanol gave **8Ni** (8.1 mg, 8.7 μmol, 87%).

8Ni: ^{1}H NMR (600 MHz, $CDCl_3$, 25 °C): δ = 8.72 (d, *J* = 5.1 Hz, 2H, *β*), 8.45 (s, 1H, *meso*), 8.33 (d, *J* = 5.1 Hz, 2H, *β*), 7.87 (d, *J* = 1.4 Hz, 2H, Ar), 7.86 (d, *J* = 1.4 Hz, 2H, Ar), 7.79 (s, 2H, *β*), 7.71 (t, *J* = 1.4 Hz, 1H, Ar), 7.06 (d, *J* = 1.4 Hz, 2H, Ar), 1.59 (s, 18H, *tert*-butyl), 1.55 (s, 18H, *tert*-butyl), and 1.47 (s, 18H, *tert*-butyl) ppm; ^{13}C NMR (151 MHz, $CDCl_3$, 25 °C): δ = 154.42, 151.55, 149.63, 149.05, 146.64, 146.53, 146.42, 144.93, 141.09, 137.36, 134.19, 133.36, 129.72, 127.91, 126.95, 126.69, 123.06, 121.50, 120.47, 115.52, 105.01 35.43, 35.17, 35.15, 31.88, 31.39, and 29.32 ppm; APCI-TOF-MS: *m*/*z* = 926.4816. Calcd for $C_{62}H_{68}N_4{}^{58}Ni$: 926.4803 $[M]^+$; UV/Vis (CH_2Cl_2): λ_{max} (ε [$M^{-1}cm^{-1}$]) = 387 (3.89 × 10^4), 439 (6.35 × 10^4), 504 (6.68 × 10^4), 614 (4.44 × 10^3), 674 (5.77 × 10^3), 720 (4.30 × 10^3), and 812 nm (2.18 × 10^3).

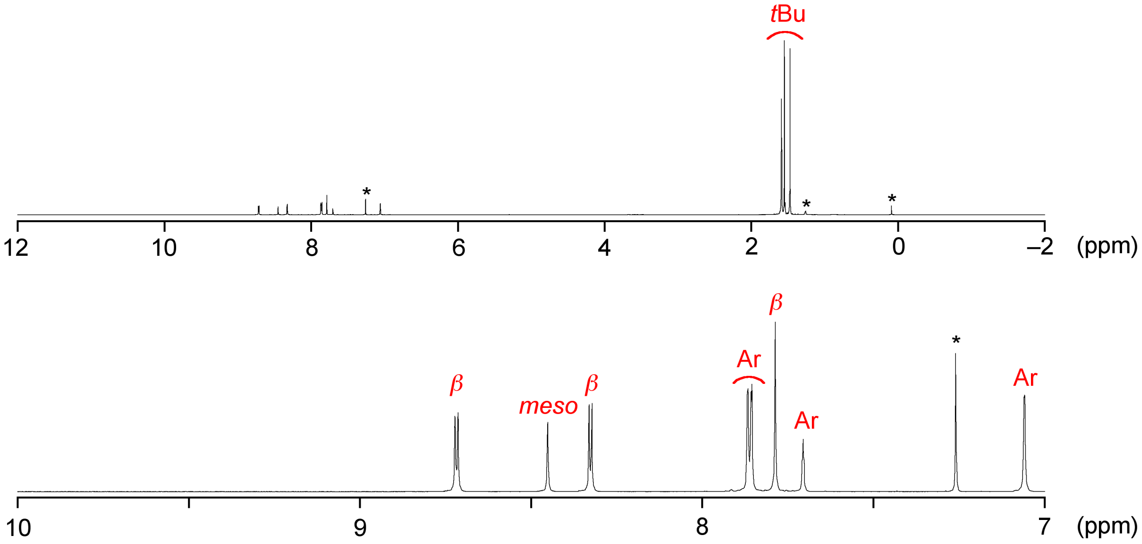

Figure S 29. ^{1}H NMR spectrum of **8Ni** in $CDCl_3$ at 25 °C. *Solvent and impurities.

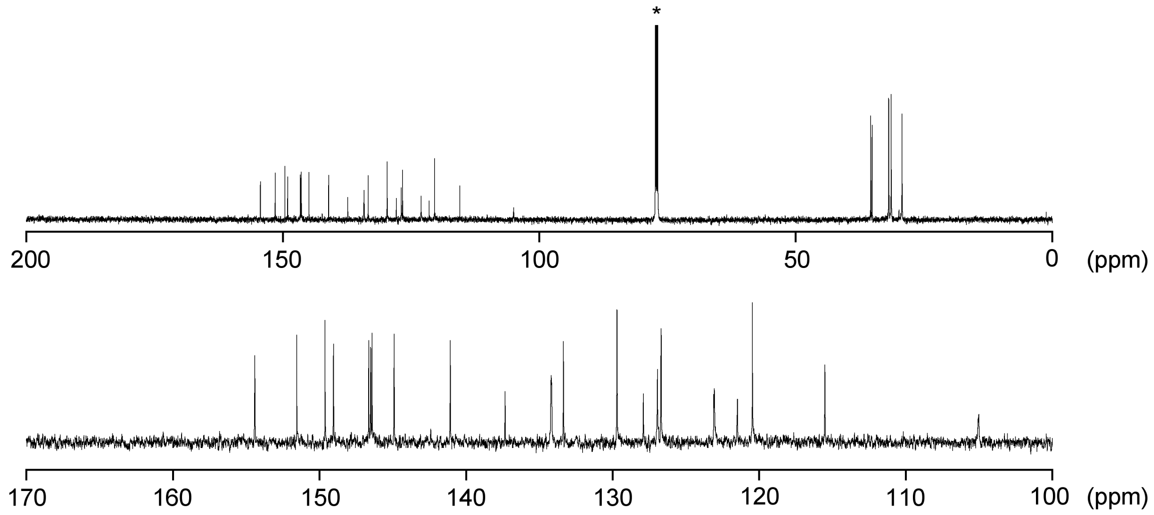

Figure S 30. ^{13}C NMR spectrum of **8Ni** in CDCl$_3$ at 25 °C. *Solvent.

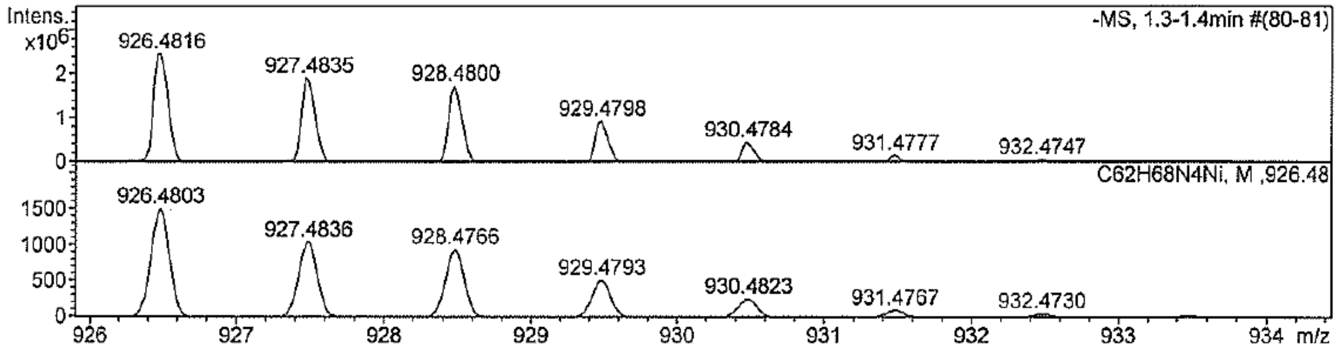

Figure S 31. Observed (top) and simulated (bottom) HR-APCI-TOF MS of **8Ni**.

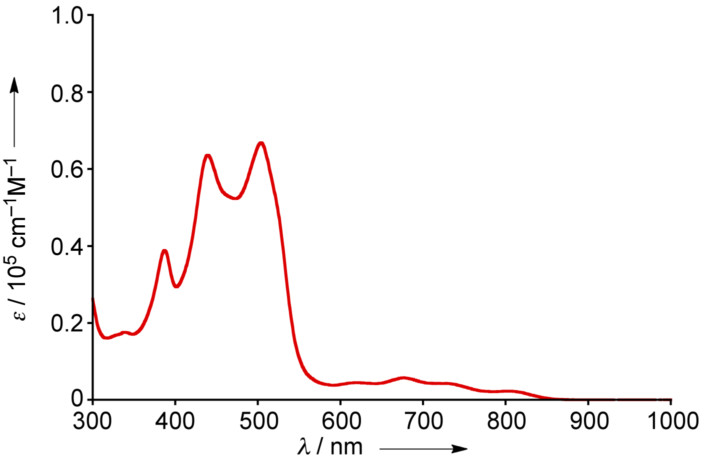

Figure S 32. UV / Vis absorption spectrum of **8Ni** in CH$_2$Cl$_2$.

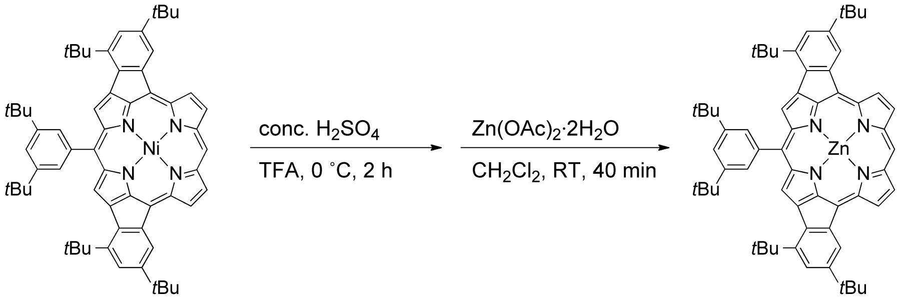

8Ni **8Zn**: 21%

Synthesis of 8Zn: Conc. H_2SO_4 (2.0 mL) was added slowly to a mixture of **8Ni** (8.4 mg, 9.1 µmol) and TFA (2.0 mL) at 0 ˚C. The reaction mixture was stirred at 0 ˚C in air for 2 h, and then poured into water at 0 ˚C. After neutralization by K_2CO_3 at 0 ˚C, the product was extracted with CH_2Cl_2, washed with brine, and dried over anhydrous Na_2SO_4. After removal of the solvent *in vacuo*, the residue was separated by silica gel chromatography eluting with CH_2Cl_2/hexane. After removal of the solvent *in vacuo*, the residue was dissolved in CH_2Cl_2, and charged with an excess amount of $Zn(OAc)_2 \cdot 2H_2O$ dissolved in MeOH. The mixture was stirred for 40 min at room temperature. After removal of the solvent *in vacuo*, the residue was separated by silica gel chromatography eluting with CH_2Cl_2/hexane. Recrystallization from CH_2Cl_2/MeCN gave **8Zn** (1.8 mg, 1.9 µmol, 21%).

8Zn: ^{1}H NMR (600 MHz, $CDCl_3$, 25 °C): δ = 8.81 (d, *J* = 4.6 Hz, 2H, β), 8.55 (s, 1H, *meso*), 8.44 (d, *J* = 4.6 Hz, 2H, β), 7.95 (d, *J* = 1.8 Hz, 2H, Ar), 7.93 (d, *J* = 1.8 Hz, 2H, Ar), 7.73 (s, 2H, β), 7.71 (t, *J* = 1.8 Hz, 1H, Ar), 7.02 (d, *J* = 1.8 Hz, 2H, Ar), 1.62 (s, 18H, *tert*-butyl), 1.57 (s, 18H, *tert*-butyl), and 1.49 (s, 18H, *tert*-butyl) ppm; ^{13}C NMR (151 MHz, $CDCl_3$, 25 °C): δ = 161.05, 154.71, 151.61, 151.06, 150.92, 149.50, 146.69, 146.62, 145.38, 138.52, 134.21, 133.45, 130.64, 130.28, 126.96, 126.83, 123.07, 121.18, 120.65, 116.25, 104.39, 35.44, 35.17, 35.13, 31.95, 31.37, and 29.36 ppm; APCI-TOF-MS: *m*/*z* = 932.4734. Calcd for $C_{62}H_{68}N_4{}^{64}Zn$: 932.4741 $[M]^{-}$; UV/Vis/NIR (CH_2Cl_2 + pyridine 1%): λ_{max} (ε [$M^{-1}cm^{-1}$]) = 426 (5.05×10^4), 503 (5.51×10^4), 528 (5.30×10^4), 596 (6.13×10^3), and 768 nm (6.84×10^3).

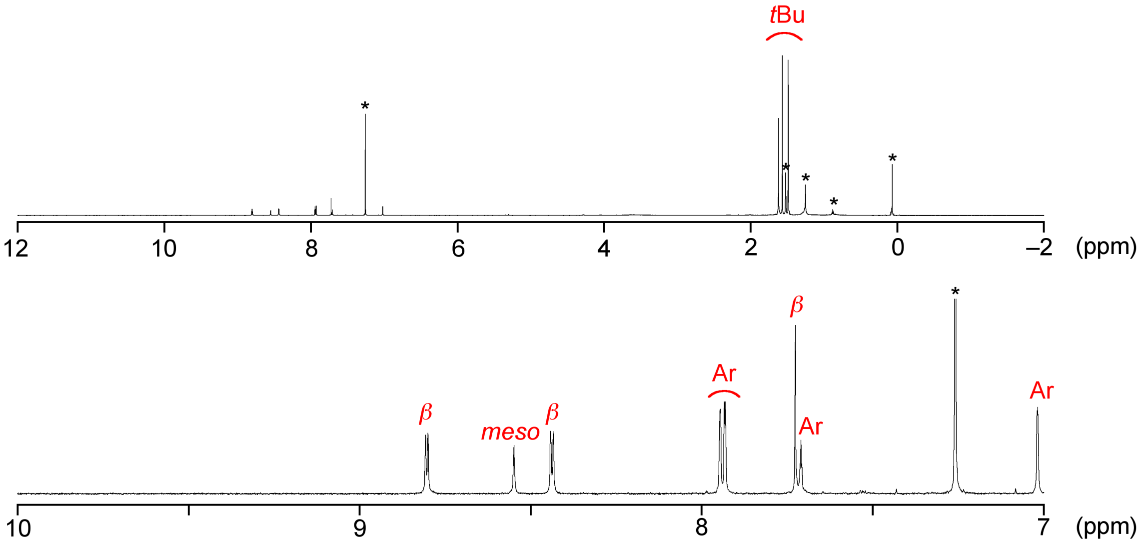

Figure S 33. ^{1}H NMR spectrum of **8Zn** in $CDCl_3$ at 25 °C. *Solvent and impurities.

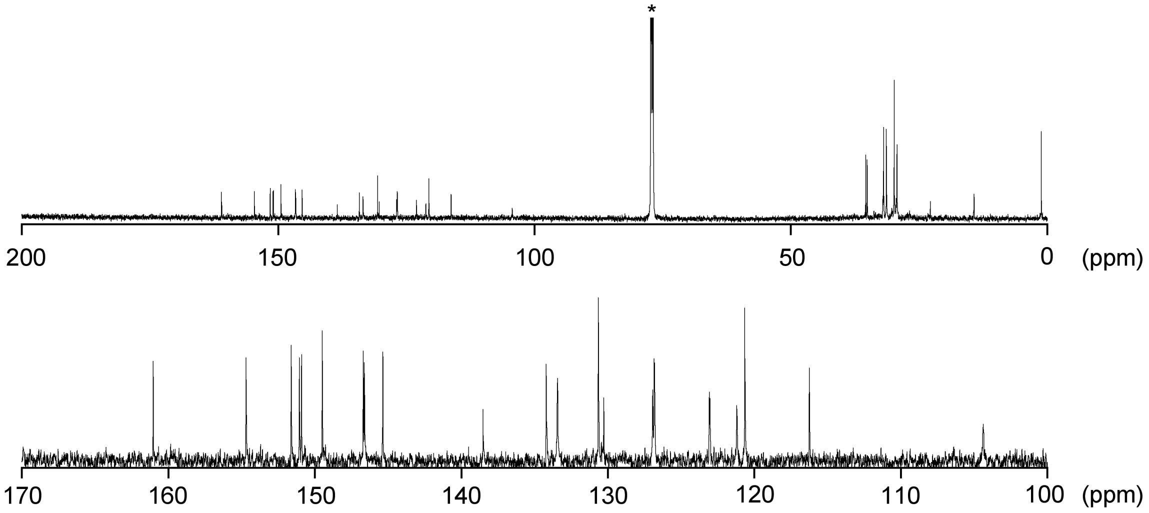

Figure S 34. ^{13}C NMR spectrum of **8Zn** in CDCl$_3$ at 25 °C. *Solvent.

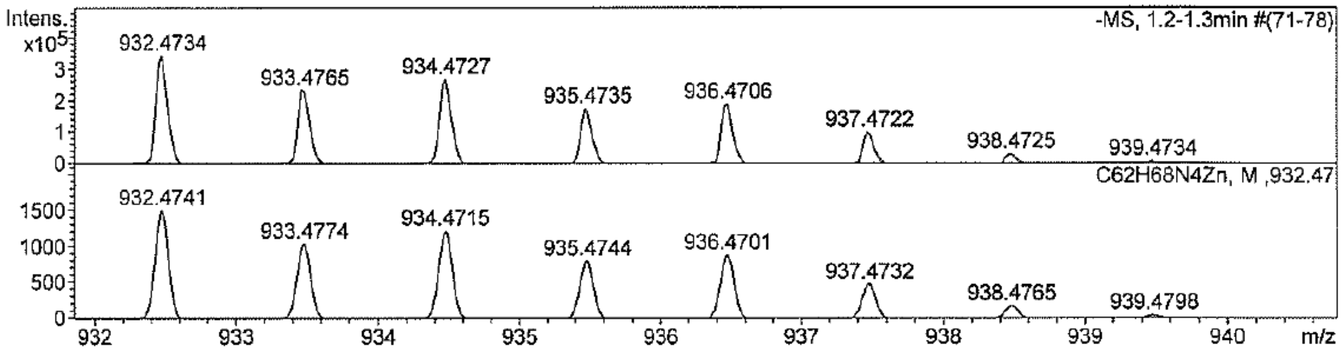

Figure S 35. Observed (top) and simulated (bottom) HR-APCI-TOF MS of **8Zn**.

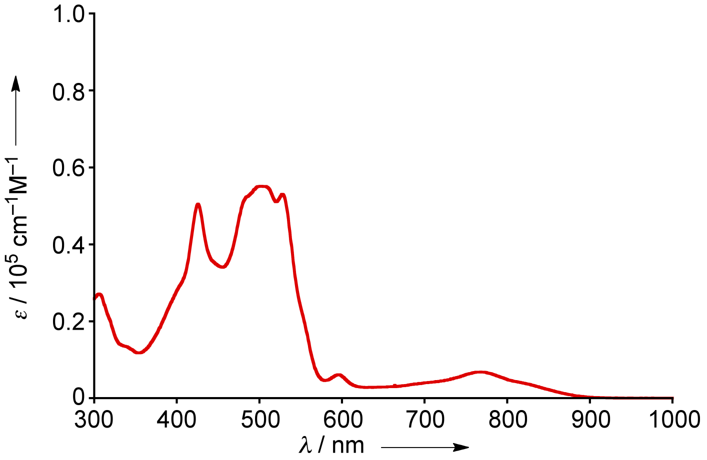

Figure S 36 .UV / Vis absorption spectrum of **8Zn** in CH$_2$Cl$_2$ containing 1% of pyridine.

4. X-Ray Crystal Structures

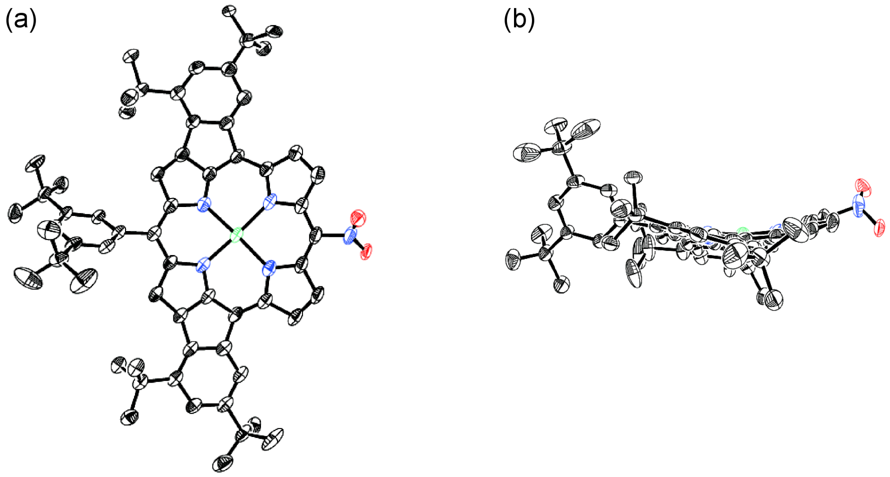

Figure S 37. X-Ray crystal structure of **2e**. (a) Top view and (b) side view. Thermal ellipsoids are shown at the 50% probability level. Solvent molecules and all hydrogen atoms are omitted for clarity.

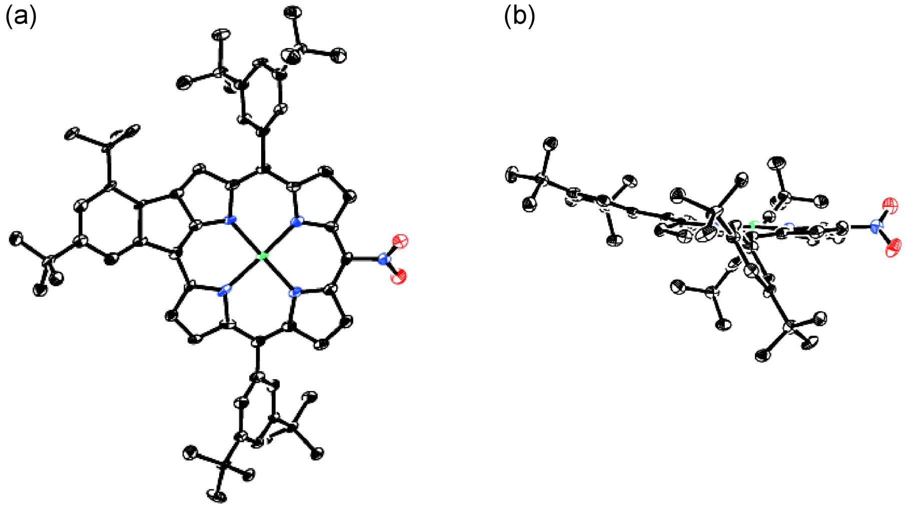

Figure S 38. X-Ray crystal structure of **3**. (a) Top view and (b) side view. Thermal ellipsoids are shown at the 50% probability level. Solvent molecules and all hydrogen atoms are omitted for clarity.

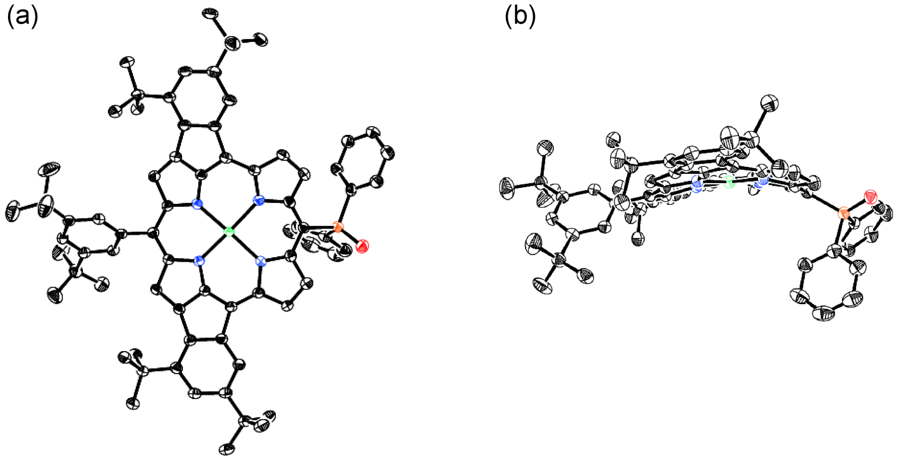

Figure S 39. X-Ray crystal structure of **2f**. (a) Top view and (b) side view. Thermal ellipsoids are shown at the 50% probability level. Solvent molecules and all hydrogen atoms are omitted for clarity.

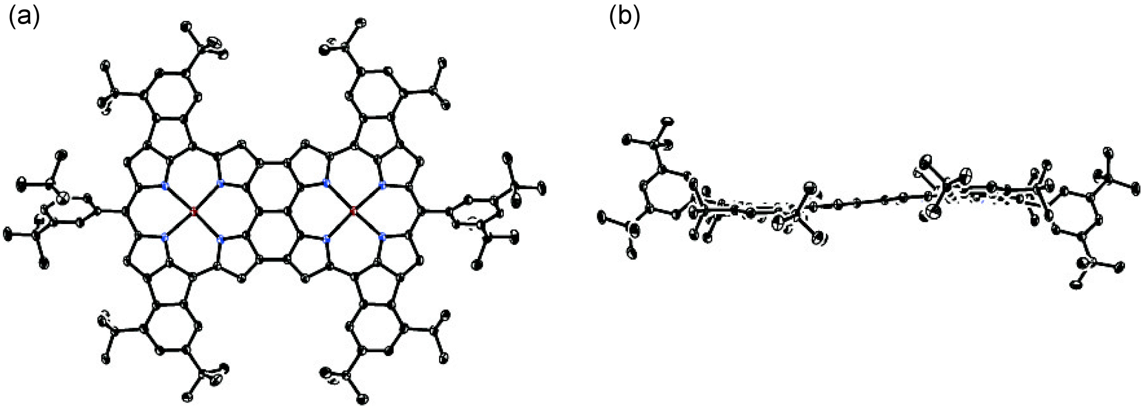

Figure S 40. X-Ray crystal structure of **6**. (a) Top view and (b) side view. Thermal ellipsoids are shown at the 50% probability level. Solvent molecules, pyridine ligands, and all hydrogen atoms are omitted for clarity.

Table S 1. Crystal data and structure refinements for **2e**, **3**, **2f**, and **6**.

Compound	**2e**	**3**	**2f**	**6**
Empirical Formula	$C_{62}H_{67}N_5O_2Ni \cdot (CHCl_3)_2$	$C_{62}H_{69}N_5O_2Ni \cdot C_7H_8$	$C_{74}H_{77}N_4OPNi \cdot C_7H_8 \cdot (C_2H_6O)_{1.5}$	$C_{124}H_{130}N_8Zn_2 \cdot (C_5H_5N)_2 \cdot (C_7H_8)_3 \cdot C_2H_3N$
Solvent System	$CHCl_3$/MeOH	toluene/EtOH	toluene/EtOH	toluene/MeCN/pyridine
Fw	1269.82	1067.05	1128.08	2349.63
Crystal System	Orthorhombic	Triclinic	Monoclinic	Triclinic
Space Group	*P*bcn (No. 60)	*P*-1 (No. 2)	*P*2_1/n (No. 14)	*P*-1 (No. 2)
a	11.0983(14) Å	14.734(6) Å	12.3714(16) Å	10.0013(12) Å
b	34.992(5) Å	20.554(8) Å	28.233(3) Å	14.5831(10) Å
c	32.965(4) Å	20.788(9) Å	41.360(6) Å	24.366(4) Å
α	90°	90.073(8)°	90°	75.428(16)°
β	90°	103.209(15)°	96.168(4)°	87.017(19)°
γ	90°	109.518(5)°	90°	71.26(2)°
Volume	12802(3) Å^3	5756(4) Å^3	14363(3) Å^3	3255.5(8) Å^3
Z	8	2	8	1
Density (calcd.)	1.318 g/cm^3	1.231 g/cm^3	1.174 g/cm^3	1.199 g/cm^3
Completeness	0.992	0.970	0.988	0.973
Goodness-of-fit (all data)	1.047	1.097	1.036	1.018
R_1 ($I>2\sigma(I)$)	0.0921	0.1419	0.0739	0.0531
wR_2 (all data)	0.2889	0.3713	0.2350	0.1531
CCDC No.	1433487	1433488	1433489	1433486

5. DFT Calculations

The energy calculations of **6** and **7** were carried out using the *Gaussian 09* program.[S2] The calculations were performed by the density functional theory (DFT) method with restricted B3LYP (Becke's three-parameter hybrid exchange functionals and the Lee-Yang-Parr correlation functional)[S3] level, employing basis sets 6-31G(d) for C, H, and N and LANL2DZ for Zn. *tert*-Butyl groups of non-fused 3,5-di-*tert*-butylphenyl groups were replaced with hydrogen atoms to simplify the calculations.

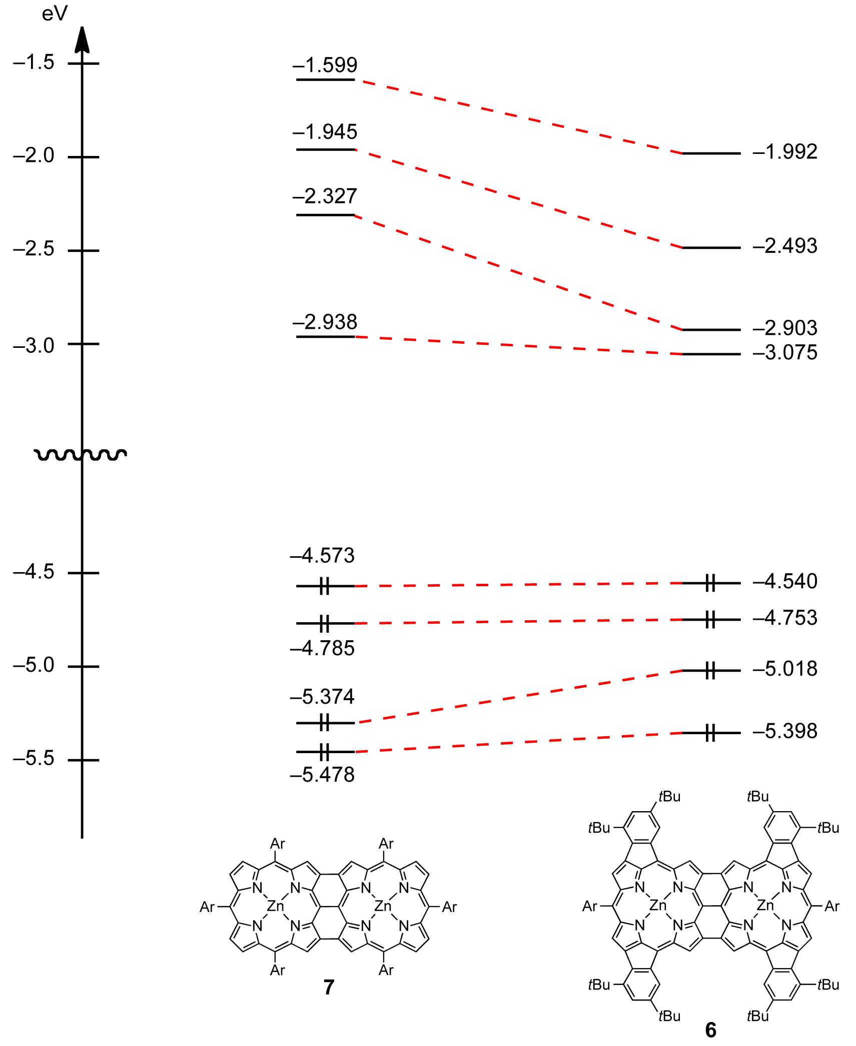

Figure S 41. Energy diagram of **6** and **7**.

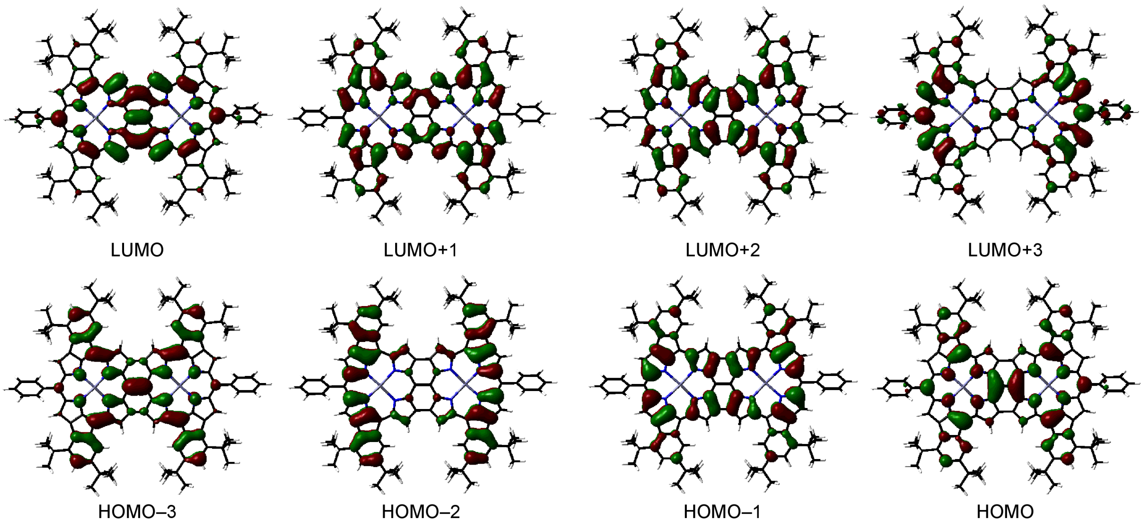

Figure S 42. Kohn-Sham orbital representations of **6**.

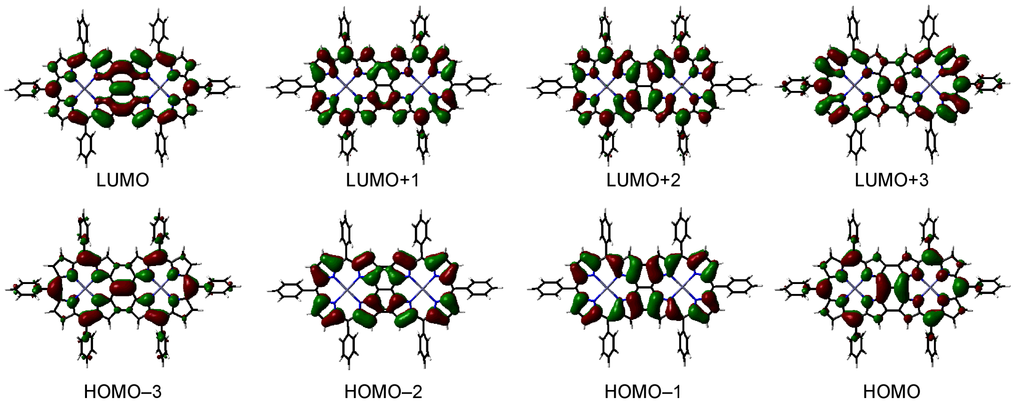

Figure S 43. Kohn-Sham orbital representations of **7**.

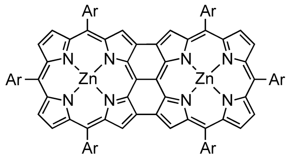

7

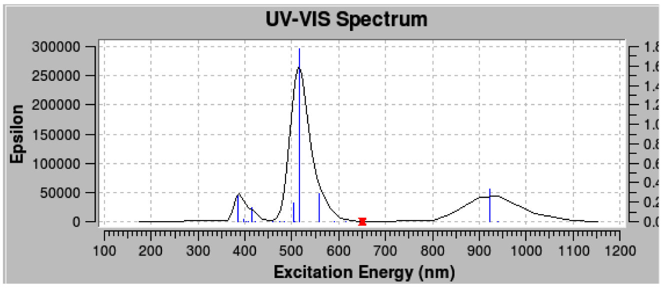

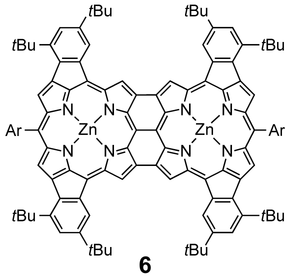

6

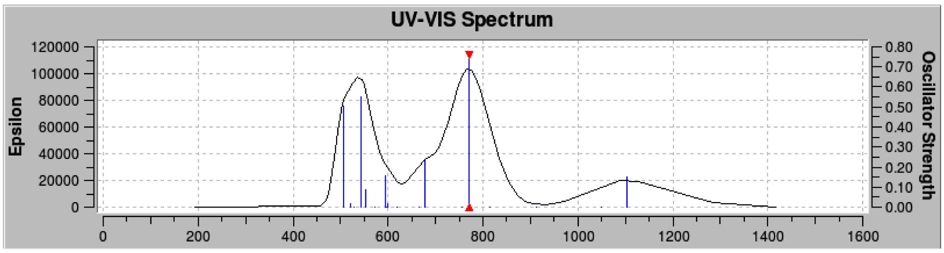

Figure S 44. Oscillator strength and simulated UV/Vis/NIR absorption spectra of **6** and **7**.

Table S 2. Selected oscillator strengths and their orbital compositions of **7**.

wavelength (nm)	oscillator strength	orbital composition			
923.48	0.3302	HOMO	to	LUMO	0.65926
		HOMO–1	to	LUMO+1	0.23175
558.79	0.2856	HOMO–1	to	LUMO+1	0.50390
		HOMO–4	to	LUMO	0.48175
515.49	1.7790	HOMO–4	to	LUMO	0.49990
		HOMO	to	LUMO	0.24463
504.90	0.1853	HOMO	to	LUMO+2	0.49355
		HOMO–2	to	LUMO	0.34305
413.90	0.1419	HOMO–2	to	LUMO+2	0.56128
		HOMO	to	LUMO+4	0.36457
		HOMO–3	to	LUMO+3	0.15636
		HOMO–5	to	LUMO+1	0.13759
385.88	0.2671	HOMO	to	LUMO+4	0.36479
		HOMO–5	to	LUMO	0.31930
		HOMO–19	to	LUMO	0.13931

Table S 3. Selected oscillator strengths and their orbital compositions of **6**.

wavelength (nm)	oscillator strength	orbital composition			
1102.77	0.1482	HOMO	to	LUMO	0.62103
770.62	0.7594	HOMO–1	to	LUMO+1	0.59574
		HOMO	to	LUMO	0.30097
		HOMO–4	to	LUMO+1	0.16386
		HOMO–2	to	LUMO+2	0.14420
676.97	0.2336	HOMO	to	LUMO+2	0.51821
		HOMO–8	to	LUMO	0.11015
593.61	0.1573	HOMO–2	to	LUMO+2	0.60516
		HOMO–4	to	LUMO+1	0.27934
		HOMO–7	to	LUMO+1	0.10559
543.89	0.5493	HOMO–4	to	LUMO+1	0.57011
505.87	0.5057	HOMO–7	to	LUMO	0.61464

The calculations of dicationic triplet states of **1e**, **1f**, and **1h**, and radical cation and dicationic singlet state of **1e** were carried out using the *Gaussian 09* program.[S2] The calculations were performed by the density functional theory (DFT) method with restricted B3LYP (Becke's three-parameter hybrid exchange functionals and the Lee-Yang-Parr correlation functional)[S3] level, employing basis sets 6-311G(d). *tert*-Butyl groups were replaced with hydrogen atoms to simplify the calculations.

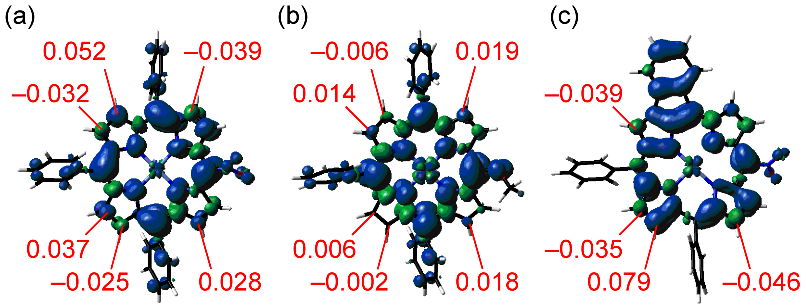

Figure S 45. Total spin density of radical cations of (a) **1e**, (b) **1h**, and (c) **4** (isovalue: 0.001).

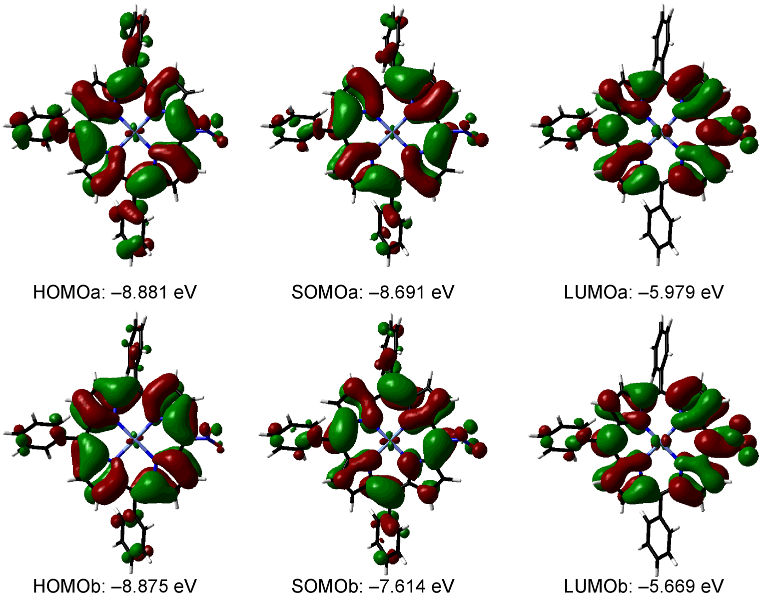

Figure S 46. Kohn-Sham orbital representations of radical cation of **1e**.

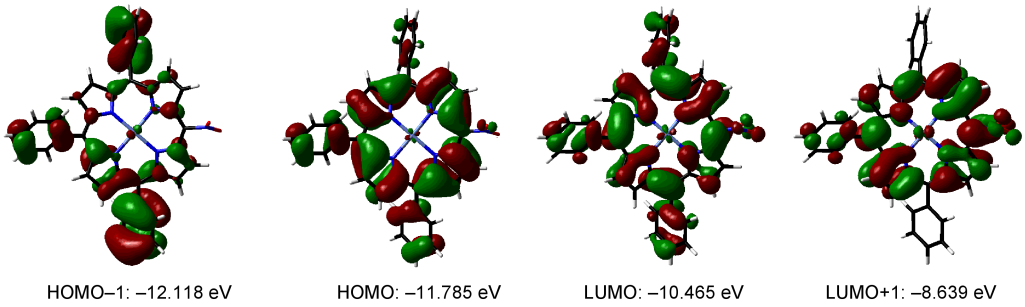

Figure S 47. Kohn-Sham orbital representations of dicationic singlet state of **1e**.

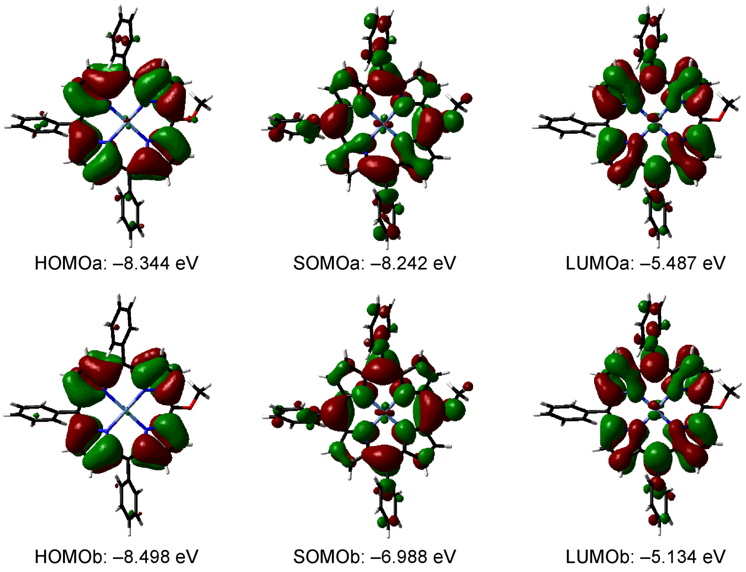

Figure S 48. Kohn-Sham orbital representations of radical cation of **1h**.

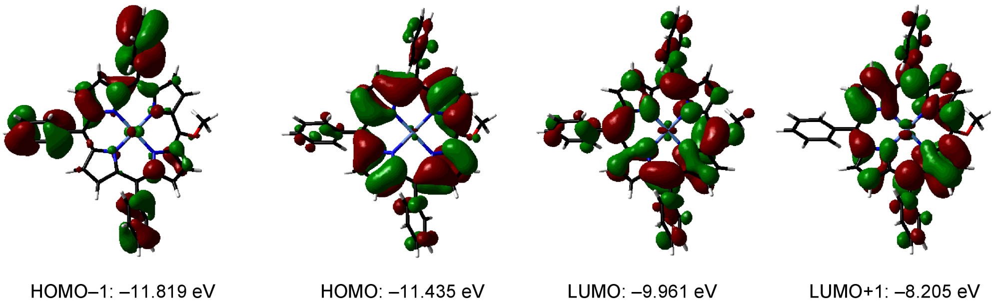

Figure S 49. Kohn-Sham orbital representations of dicationic singlet state of **1h**.

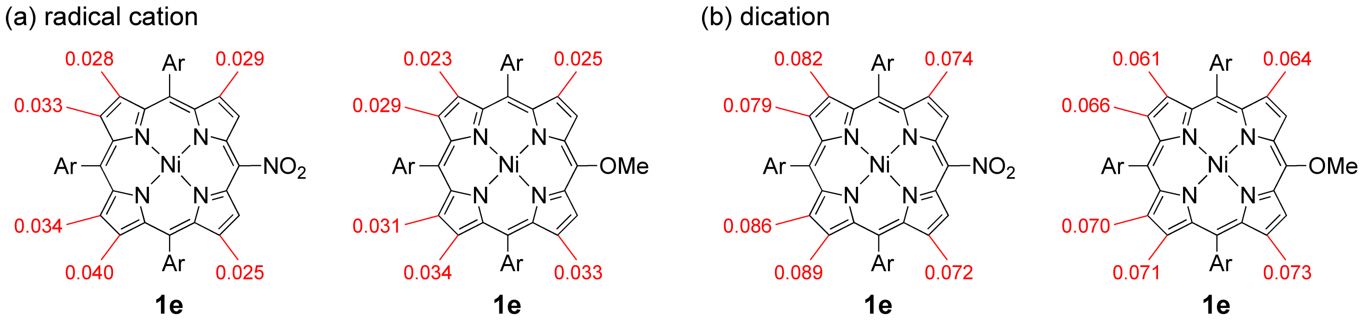

Figure S 50. Selected charge distributions of radical cations and dications of **1e** and **1h**.

6. Femtosecond Transient Absorption Measurements

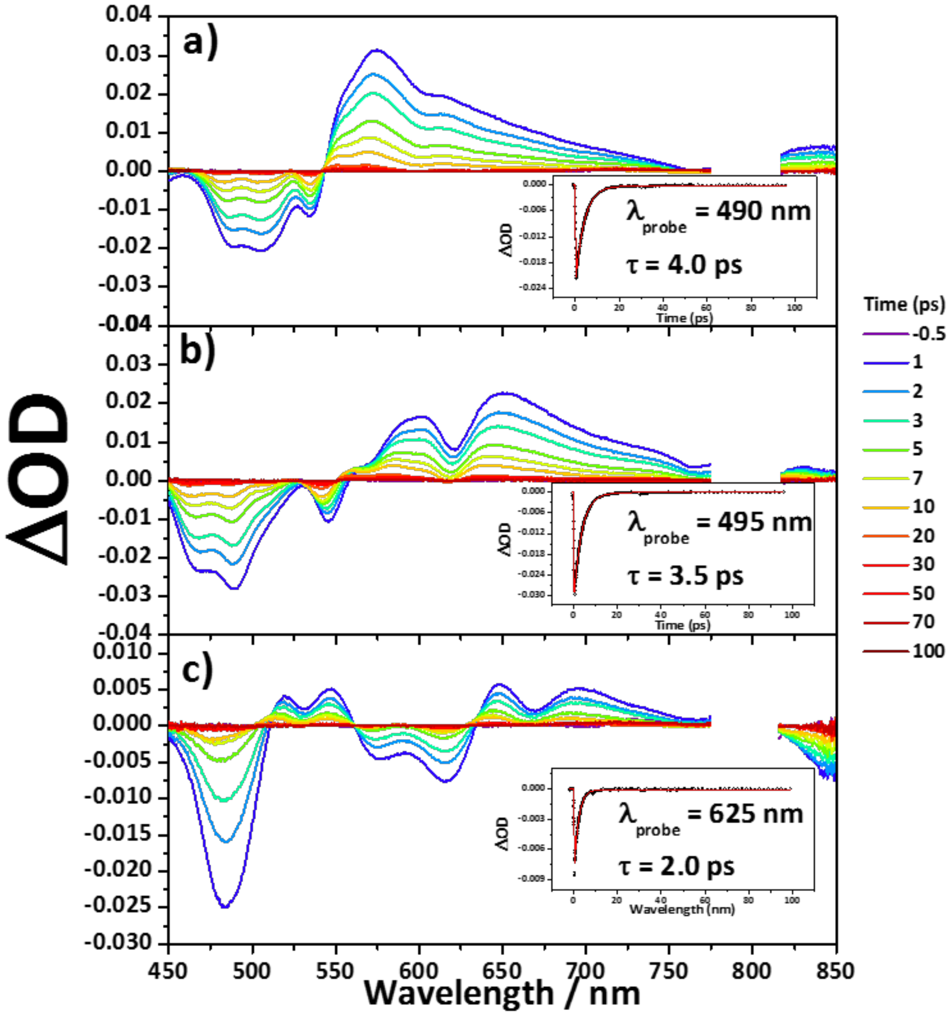

Figure S 51. Femtosecond transient absorption spectra and decay profiles (inset) of (a) **8Zn**, (b) **5Zn**, and (c) **6** in toluene containing 1% of pyridine with photoexcitation at 800 nm (for **8Zn** and **5Zn**), and 1350 nm (for **6**).

7. TPA Spectra and Z-Scan Curves

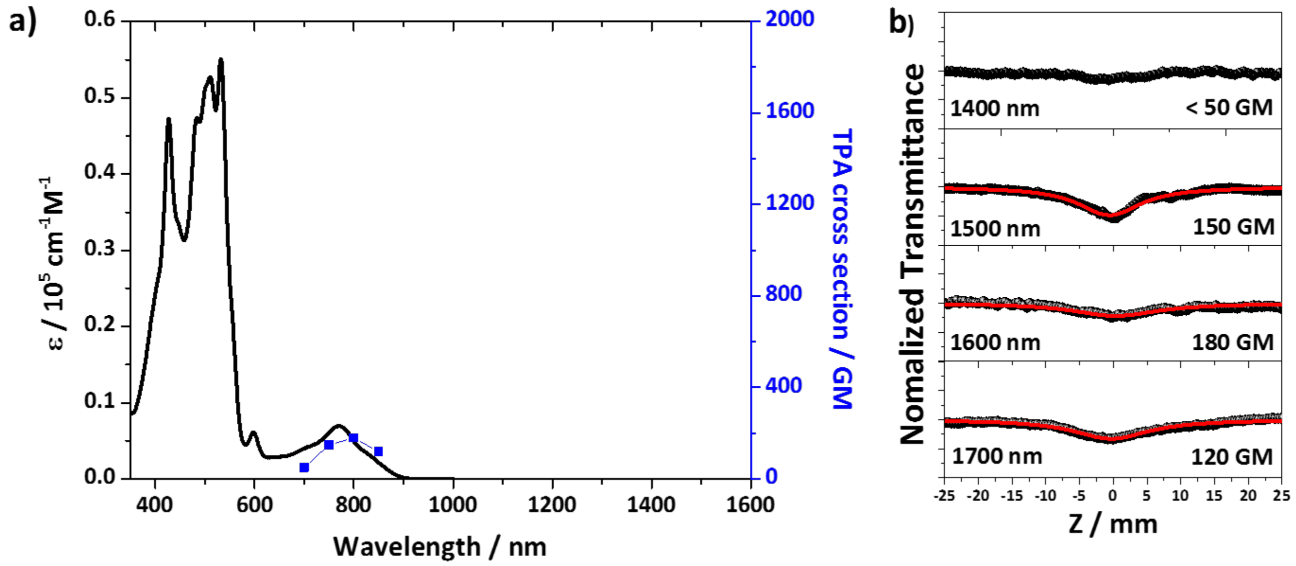

Figure S 52. (a) One-photon absorption (black) and TPA spectrum (blue) of **8Zn** . (b) Z-scan curves of **8Zn** by photoexcitations in the range from 1400 to 1700 nm in toluene containing 1% of pyridine. The TPA spectra are displayed at $\lambda_{ex}/2$ for comparison with the OPA spectra.

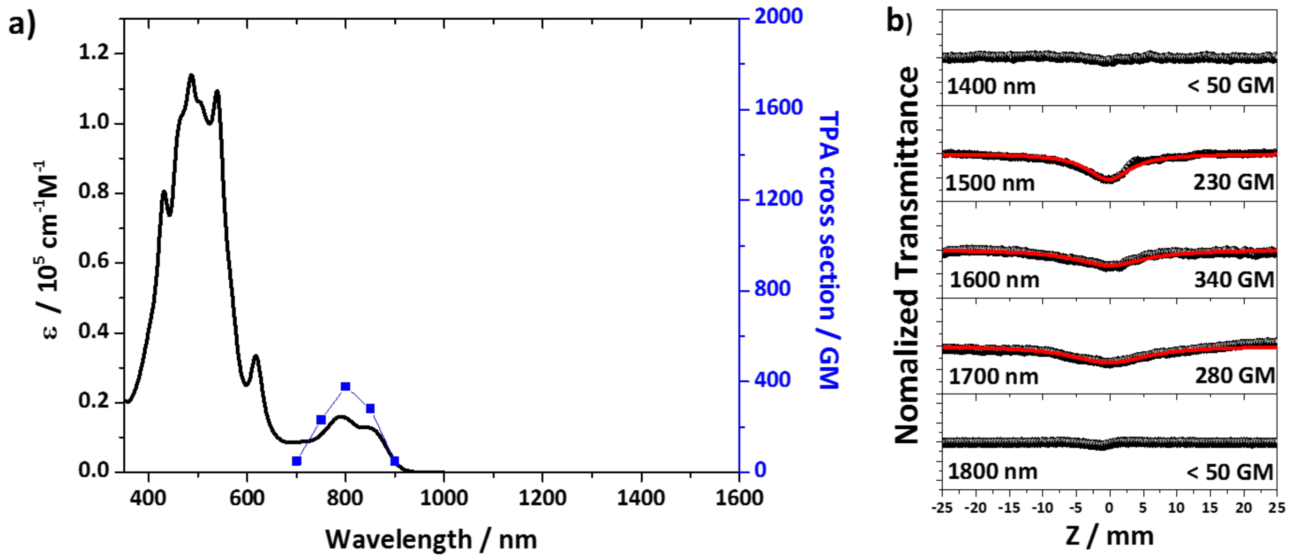

Figure S 53. (a) One-photon absorption (black) and TPA spectrum (blue) of **5Zn**. (b) Z-scan curves of **5Zn** by photoexcitations in the range from 1400 to 1800 nm in toluene containing 1% of pyridine. The TPA spectra are displayed at $\lambda_{ex}/2$ for comparison with the OPA spectra.

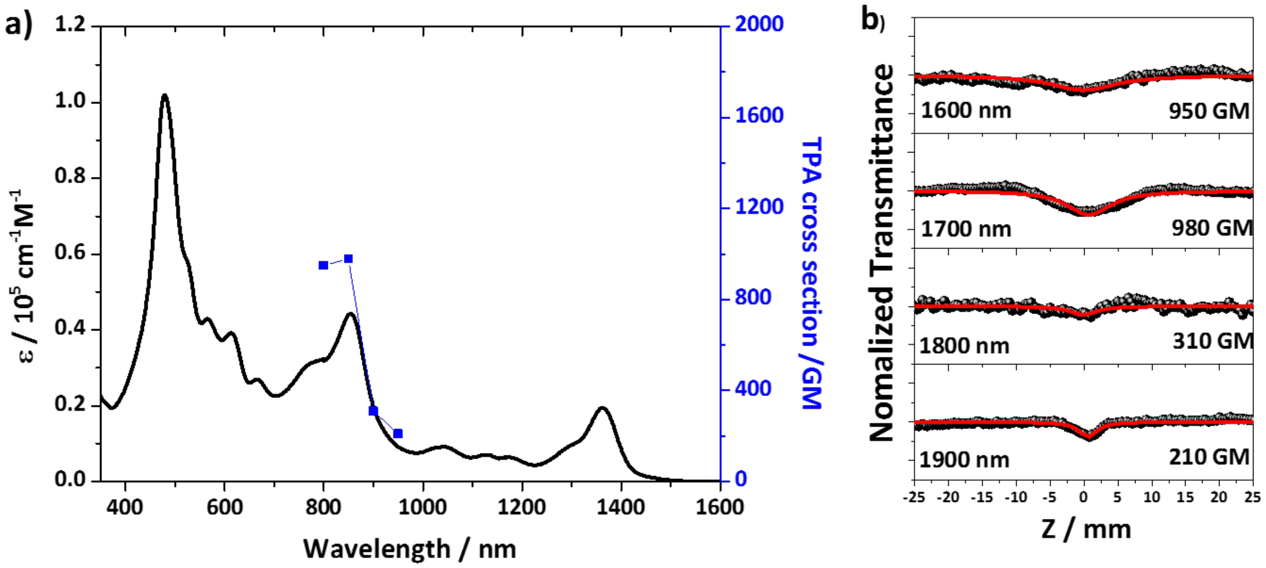

Figure S 54. (a) One-photon absorption (black) and TPA spectrum (blue) of **6**. (b) Z-scan curves of **6** by photoexcitations in the range from 1600 to 1900 nm in toluene containing 1% of pyridine. The TPA spectra are displayed at $\lambda_{ex}/2$ for comparison with the OPA spectra.

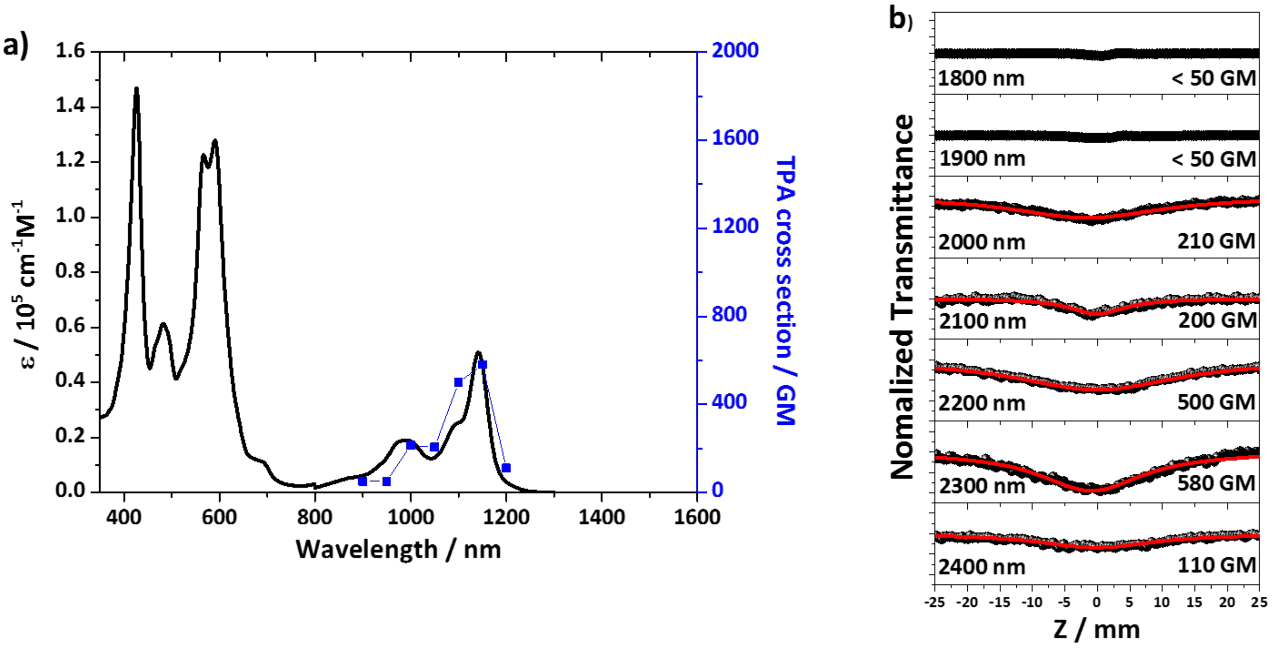

Figure S 55. (a) One-photon absorption (black) and TPA spectrum (blue) of **7**. (b) Z-scan curves of **7** by photoexcitations in the range from 1800 to 2400 nm in toluene containing 1% of pyridine. The TPA spectra are displayed at $\lambda_{ex}/2$ for comparison with the OPA spectra.

8. NICS Calculations and ACID Plot

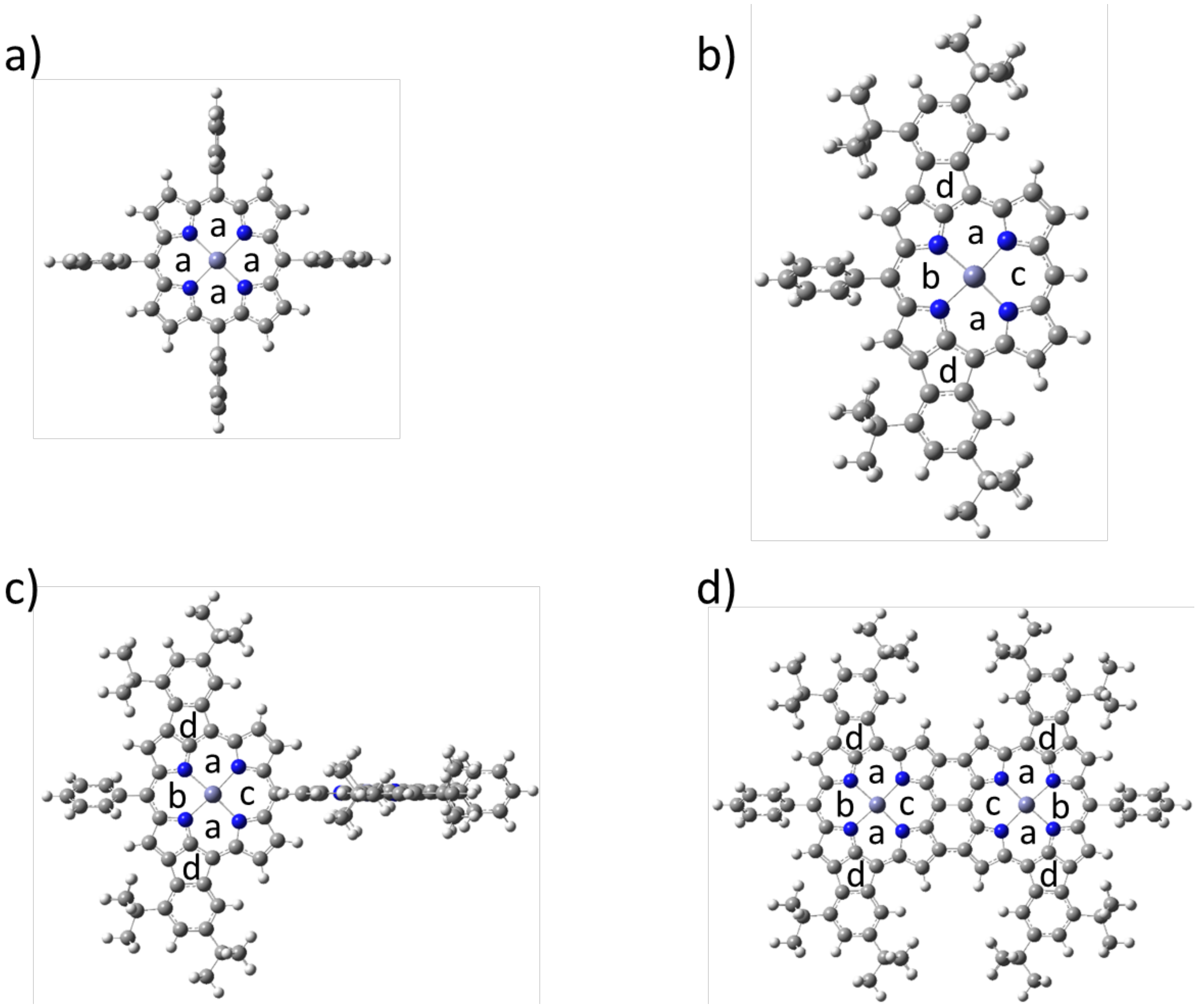

Figure S 56. Calculated NICS(0) positions of (a) **ZnTPP**, (b) **8Zn,** (c) **5Zn**, (d) and **6**.

Table S 4. Calculated NICS(0) values at the positions (Figure S 50) of **ZnTPP**, **8Zn**, **5Zn**, and **6**

	NICS(0) value (ppm)			
	a	b	c	d
ZnTPP	-16.6	-	-	-
8Zn	-12.3	-9.7	-11.4	17.0
5Zn	-11.7	-9.3	-9.8	17.0
6	-4.3	-1.7	-5.9	11.7

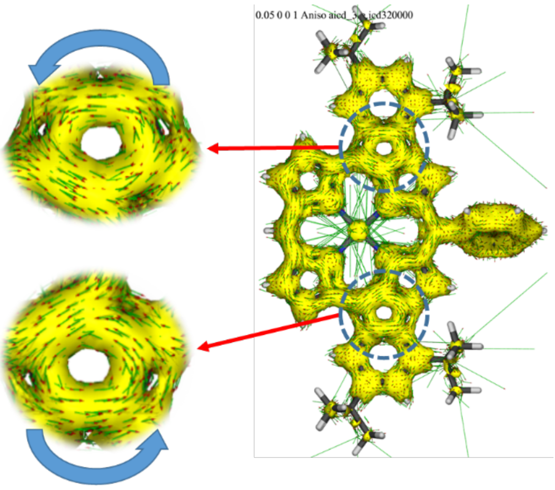

Figure S 57. Anisotropy of induced current density (ACID) plot for **8Zn** at an isosurface value of 0.05 at the B3LYP/6-31G(d) level.

9. Electrochemical Properties

Cyclic voltammograms and differential pulse voltammograms were obtained under the following conditions; solvent: CH_2Cl_2 containing 1% pyridine, electrolyte: 0.1 M $n$$Bu_4NPF_6$, working electrode: glassy carbon, counter electrode: Pt, reference electrode: Ag/$AgNO_3$, scan rate: 0.05 mV/s.

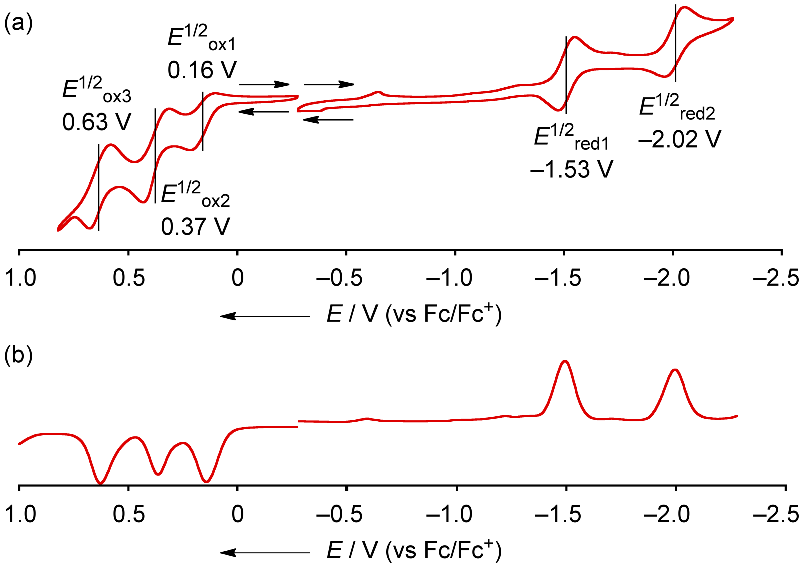

Figure S 58. (a) Cyclic voltammograms and (b) differential pulse voltammograms of **8Zn**.

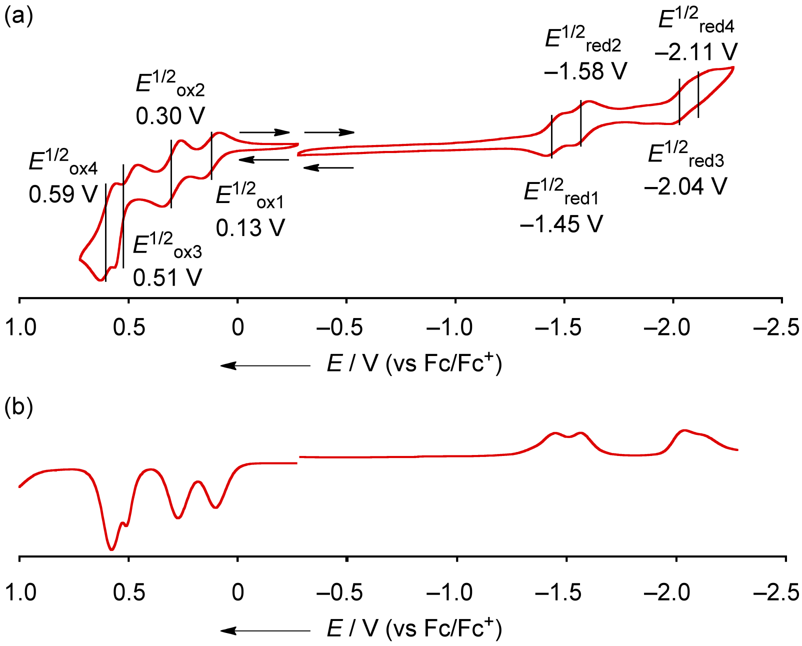

Figure S 59. (a) Cyclic voltammograms and (b) differential pulse voltammograms of **5Zn**.

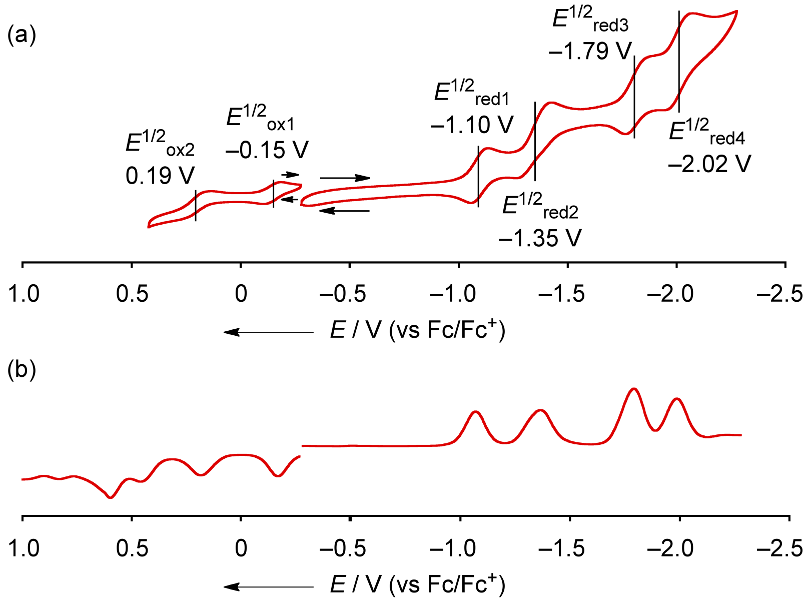

Figure S 60. (a) Cyclic voltammograms and (b) differential pulse voltammograms of **6**.

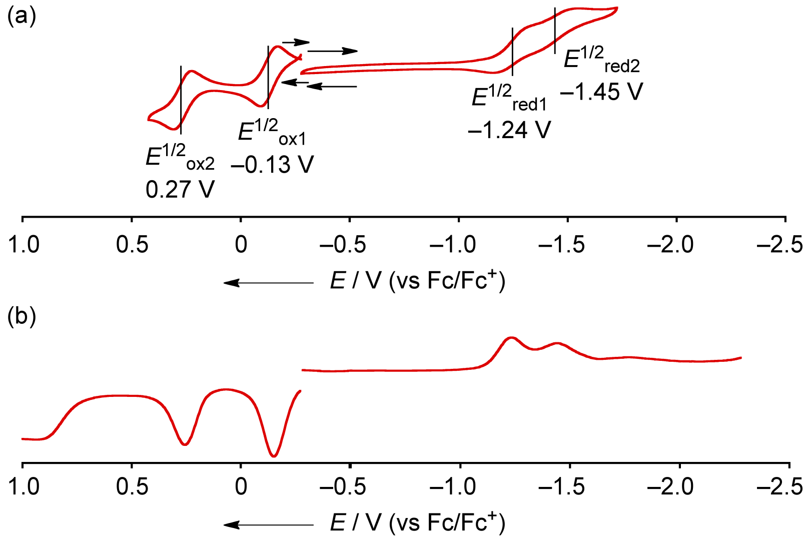

Figure S 61. (a) Cyclic voltammograms and (b) differential pulse voltammograms of **7**.

10. References

[S1] SHELXL-97 and SHELXS-97, program for refinement of crystal structures from diffraction data, University of Goettingen, Göttingen (Germany); G. Sheldrick and T. Schneider, *Methods Enzymol.* 1997, **277**, 319.

[S2] Gaussian 09, Revision A.02, M. J. Frisch, G. W. Trucks, H. B. Schlegel, G. E. Scuseria, M. A. Robb, J. R. Cheeseman, G. Scalmani, V. Barone, B. Mennucci, G. A. Petersson, H. Nakatsuji, M. Caricato, X. Li, H. P. Hratchian, A. F. Izmaylov, J. Bloino, G. Zheng, J. L. Sonnenberg, M. Hada, M. Ehara, K. Toyota, R. Fukuda, J. Hasegawa, M. Ishida, T. Nakajima, Y. Honda, O. Kitao, H. Nakai, T. Vreven, J. A. Montgomery, Jr., J. E. Peralta, F. Ogliaro, M. Bearpark, J. J. Heyd, E. Brothers, K. N. Kudin, V. N. Staroverov, R. Kobayashi, J. Normand, K. Raghavachari, A. Rendell, J. C. Burant, S. S. Iyengar, J. Tomasi, M. Cossi, N. Rega, J. M. Millam, M. Klene, J. E. Knox, J. B. Cross, V. Bakken, C. Adamo, J. Jaramillo, R. Gomperts, R. E. Stratmann, O. Yazyev, A. J. Austin, R. Cammi, C. Pomelli, J. W. Ochterski, R. L. Martin, K. Morokuma, V. G. Zakrzewski, G. A. Voth, P. Salvador, J. J. Dannenberg, S. Dapprich, A. D. Daniels, O. Farkas, J. B. Foresman, J. V. Ortiz, J. Cioslowski and D. J. Fox, Gaussian, Inc.: Wallingford, CT, 2009.

[S3] a) A. D. Becke, *J. Chem. Phys.* 1993, **98**, 1372; b) C. Lee, W. Yang and R. G. Parr, *Phys. Rev. B* 1998, **37**, 785.